the plant journal

SEB SOCIETY FOR EXPERIMENTAL BIOLOGY

The Plant Journal (2021) doi: 10.1111/tpj.15384

Time-series transcriptomics reveals a *BBX32*-directed control of acclimation to high light in mature *Arabidopsis* leaves

Ruben Alvarez-Fernandez[1,†], Christopher A. Penfold[2,‡], Gregorio Galvez-Valdivieso[1,§], Marino Exposito-Rodriguez[1], Ellie J. Stallard[1], Laura Bowden[3,¶], Jonathan D. Moore[3,#], Andrew Mead[3,††], Phillip A. Davey[1], Jack S. A. Matthews[1], Jim Beynon[2], Vicky Buchanan-Wollaston[3], David L. Wild[2], Tracy Lawson[1], Ulrike Bechtold[1], Katherine J. Denby[4] and Philip M. Mullineaux[1,*]

[1]*School of Life Sciences, University of Essex, Wivenhoe Park, Colchester, Essex CO4 3SQ, UK,*
[2]*Department of Statistics, Warwick University, Coventry CV4 7AL, UK,*
[3]*School of Life Sciences, Warwick University, Coventry CV4 7AL, UK, and*
[4]*Centre for Novel Agricultural Products (CNAP), Department of Biology, University of York, Wentworth Way, York YO10 5DD, UK*

Received 20 May 2021; accepted 14 June 2021.
*For correspondence (e-mail mullin@essex.ac.uk).
[†]Present address: Phoremost Ltd, Building 250, Babraham Research Campus, Cambridgeshire, CB22 3AT, UK
[‡]Present address: Department of Physiology, Development and Neuroscience, University of Cambridge, Downing Site, Cambridge, CB2 3EG, UK
[§]Present address: Departamento de Botánica, Ecología y Fisiología Vegetal, Instituto Andaluz de Biotecnología and Campus Agroalimentario de Excelencia Internacional ceiA3, Campus de Rabanales, Edif. C-6, 1ª Planta, Universidad de Córdoba, Córdoba, 14071, Spain
[¶]Present address: Science and Advice for Scottish Agriculture, Roddinglaw Road, Edinburgh, EH12 9FJ, UK
[#]Present address: John Innes Centre, Norwich Research Park, Colney, Norwich, NR4 7UH, UK
[††]Present address: Computational and Analytical Sciences, Rothamsted Research, Harpenden, Hertfordshire, AL5 2JQ, UK

SUMMARY

The photosynthetic capacity of mature leaves increases after several days' exposure to constant or intermittent episodes of high light (HL) and is manifested primarily as changes in chloroplast physiology. How this chloroplast-level acclimation to HL is initiated and controlled is unknown. From expanded Arabidopsis leaves, we determined HL-dependent changes in transcript abundance of 3844 genes in a 0–6 h time-series transcriptomics experiment. It was hypothesized that among such genes were those that contribute to the initiation of HL acclimation. By focusing on differentially expressed transcription (co-)factor genes and applying dynamic statistical modelling to the temporal transcriptomics data, a regulatory network of 47 predominantly photoreceptor-regulated transcription (co-)factor genes was inferred. The most connected gene in this network was *B-BOX DOMAIN CONTAINING PROTEIN32* (*BBX32*). Plants overexpressing *BBX32* were strongly impaired in acclimation to HL and displayed perturbed expression of photosynthesis-associated genes under LL and after exposure to HL. These observations led to demonstrating that as well as regulation of chloroplast-level acclimation by *BBX32, CRYPTOCHROME1, LONG HYPOCOTYL5, CONSTITUTIVELY PHOTOMORPHOGENIC1* and *SUPPRESSOR OF PHYA-105* are important. In addition, the *BBX32*-centric gene regulatory network provides a view of the transcriptional control of acclimation in mature leaves distinct from other photoreceptor-regulated processes, such as seedling photomorphogenesis.

Keywords: photosynthesis, B-Box proteins, acclimation, high light, hydrogen peroxide, Arabidopsis, Bayesian dynamic statistical modelling, gene regulatory networks, transcriptomics.

INTRODUCTION

The exposure of plants to increased light intensities can lead to the development of enhanced photosynthetic capacity [here defined as high-light (HL) acclimation], is an important determinant of plant fitness or crop yield, is under genetic as well as environmental control and includes changes in the expression of many genes (Athanasiou et al., 2010; Eberhard et al., 2008; Murchie and Horton, 1997; Murchie et al., 2005; Oguchi et al., 2003; van Rooijen et al., 2015; Schottler and Toth, 2014; Vialet-Chabrand et al., 2017; Walters et al., 1999). In young expanding leaves, acclimation to HL brings about increased photosynthetic capacity by eliciting changes in both leaf morphology, such as altered leaf and vascular

diameter in minor veins and thickness of the lamina (Adams et al., 2014; Oguchi et al., 2003; Terashima et al., 2011; Vialet-Chabrand et al., 2017). This developmental acclimation includes changes to chloroplast physiology such as adjustments to the composition of reaction centres and light harvesting antennae (Drozak and Romanowska, 2006; Murchie and Horton, 1997; Murchie et al., 2005; Vialet-Chabrand et al., 2017; Walters et al., 1999). In contrast, in mature leaves, exposure to sustained or episodic HL brings about changes primarily in chloroplast physiology that raise the light use efficiency of photosynthesis, which can reflect increased rates of photosynthesis and/or a decreased number of photosystem II (PSII) reaction centres and is termed dynamic acclimation (Athanasiou et al., 2010; Murchie et al., 2005; van Rooijen et al., 2015; Vialet-Chabrand et al., 2017; Walters et al., 1999).

For both dynamic and developmental acclimation, it is not known how HL exposure initiates the process at the level of the chloroplast. However, an important lead is provided from an early study (Walters et al., 1999). This was a comparison of Arabidopsis photoreceptor signalling the photosynthetic capacity of mutants and PSII efficiency grown under two different light intensities [photosynthetically active photon flux densities (PPFDs)] of 100 and 400 μmol m^{-2} sec^{-1}. From this study, it was proposed that a *PHYTOCHROMEA* (*PHYA*), *PHYB*, and *CRYPTOCHROME1* (*CRY1*) photoreceptor driven *CONSTITUTIVELY PHOTOMORPHOGENIC/DE-ETIOLATED1/FUSCA* (*COP/DET/FUS*) regulatory module could transmit signals from the nucleus to chloroplasts to participate in establishing increased photosynthetic capacity (Walters et al., 1999). In support of this, photosynthesis-associated nuclear genes are among the most enriched gene classes subject to control from photoreceptors in de-etiolating seedlings (Chory and Peto, 1990; Ganguly et al., 2015; Holtan et al., 2011; Li et al., 2015; Pham et al., 2018; Shikata et al., 2014). Various combinations of the 11 *COP/DET/FUS* loci (Lau and Deng, 2012), in conjunction with other regulatory genes, control the integration of signals from photoreceptors and are central to many plant–light environment interactions including seedling photomorphogenesis, the shade avoidance response, stomatal opening and development, the timing of flowering and cross-talk between phytohormone and light signalling (Dong et al., 2014; Huang et al., 2014; Lau and Deng, 2012; Pham et al., 2018).

The establishment of acclimation can take up to 6 days (Athanasiou et al., 2010) and before this, plants must deal with HL by dissipating excitation energy to minimize irreversible photoinhibition. Photoinhibition is caused by oxidative damage to the photosynthetic apparatus brought about by increased production of singlet oxygen ($^1O_2$;Mullineaux et al., 2018; Ramel et al., 2013; Triantaphyllidès et al., 2008). Prevention of photoinhibition is achieved by a combination of non-photochemical and photochemical quenching (NPQ and PQ respectively; Baker, 2008; Eberhard et al., 2008; Ruban and Belgio, 2014). All leaves have an extant capability to dissipate excitation energy, which is augmented under HL by localized and systemic induction of further photo-protective NPQ and/or PQ (Eberhard et al., 2008; Galvez-Valdivieso et al., 2009; Karpinski et al., 1999; Li et al., 2009; Long et al., 1994; Ruban and Belgio, 2014; Suorsa et al., 2012). NPQ is the resonance transfer of excitation energy to xanthophyll carotenoids from excited chlorophylls and its subsequent thermal dissipation (Baker, 2008; Li et al., 2000). PQ is the dissipation of excitation energy by consumption of reducing equivalents by a range of metabolic processes including enhanced photosynthetic capacity, but is also associated with increased foliar levels of hydrogen peroxide (H_2O_2) and the superoxide anion (Badger et al., 2000; Díaz et al., 2007; Driever and Baker, 2010; Eberhard et al., 2008; Heyno et al., 2014; Kangasjärvi et al., 2012; Lawson et al., 2014; Long et al., 1994; Mullineaux et al., 2018; Schiebe, 2004; Schiebe and Dietz, 2012; Streb et al., 2005; Wingler et al., 2000).

In this study, we hypothesized that in the first hours of exposure of fully expanded leaves to HL, processes are initiated that eventually lead, several days later, to acclimation manifested as increased photosynthetic capacity. This hypothesis of an early initiation of HL acclimation processes was an extension of an earlier proposal regarding the temporal order of events leading to protection against oxidative stress-induced photoinhibition and the restructuring of light harvesting antennae and PSI/PSII reaction centres (Eberhard et al., 2008). We set out to test this hypothesis by identifying genes that would have a role in both determining immediate responses to HL and the capacity to acclimate.

RESULTS

Gene Ontology analysis of time-series transcriptomics of HL-exposed leaves provides insights into the initiation of acclimation

The starting point for this study was the development of a HL time-series transcriptomics experiment. Our plan was to subject groups of time-resolved differentially expressed genes (DEGs) to Variational Bayesian State Space Modelling (VBSSM; see Experimental procedures), which requires highly resolved time-series data (Beal et al., 2005; Bechtold et al., 2016; Penfold and Buchanan-Wollaston, 2014; Penfold and Wild, 2011). Therefore, we opted for 30-min sampling over a 6 h HL period beginning 1 h after subjective dawn. We chose this time period because it spans the initiation of both the short-term and long-term acclimation to HL proposed by Eberhard et al. (2008).

Full transcriptome profiles using CATMA microarrays (Sclep et al., 2007) were obtained from leaf 7 of HL-exposed plants along with parallel LL controls. Leaf 7 from 35 days post-germination (dpg) plants was chosen because under our growth conditions (see Experimental procedures) this leaf had ceased expansion, although the rosette continued to increase in area and biomass (Bechtold et al., 2016). Microarray analysis of variance (MAANOVA; Wu et al., 2003; see Experimental procedures) was used to extract expression values from each probe for every treatment for each technical and biological replicate. To determine DEGs that showed a significant difference between HL-exposed leaves and the LL controls over all or part of the time period, a Gaussian process two-sample test (GP2S; Stegle et al., 2010) was applied and 4069 probes were selected with a Bayes factor score >10, which corresponded to 3844 DEGs (Data S1). The full dataset is deposited with Gene Expression Omnibus (GEO; GSE78251).

To obtain further insight into the overall response to HL at the molecular level, hierarchical co-cluster analysis of the 3844 DEGs was carried out using SPLINECLUSTER (Heard et al., 2005). We reasoned that groups of DEGs that display similar temporal patterns of expression could be co-regulated and clustering would be useful in identifying groups of genes for dynamic modelling. Based on comparing temporal gene expression patterns in both the HL-exposed and control LL leaves, the 3844 DEGs were divided into 43 temporal clusters (Figure 1a; Data S1). The outcome of this co-clustering was differential transcript abundance between LL and HL conditions superimposed on a range of temporal expression trends across 6 h of the diel. Plotted examples showing a range of temporal and differential expression in six clusters can be viewed in Figure S1.

The clusters are ordered such that 1–13 show general transcript abundance to be lower in HL versus LL samples

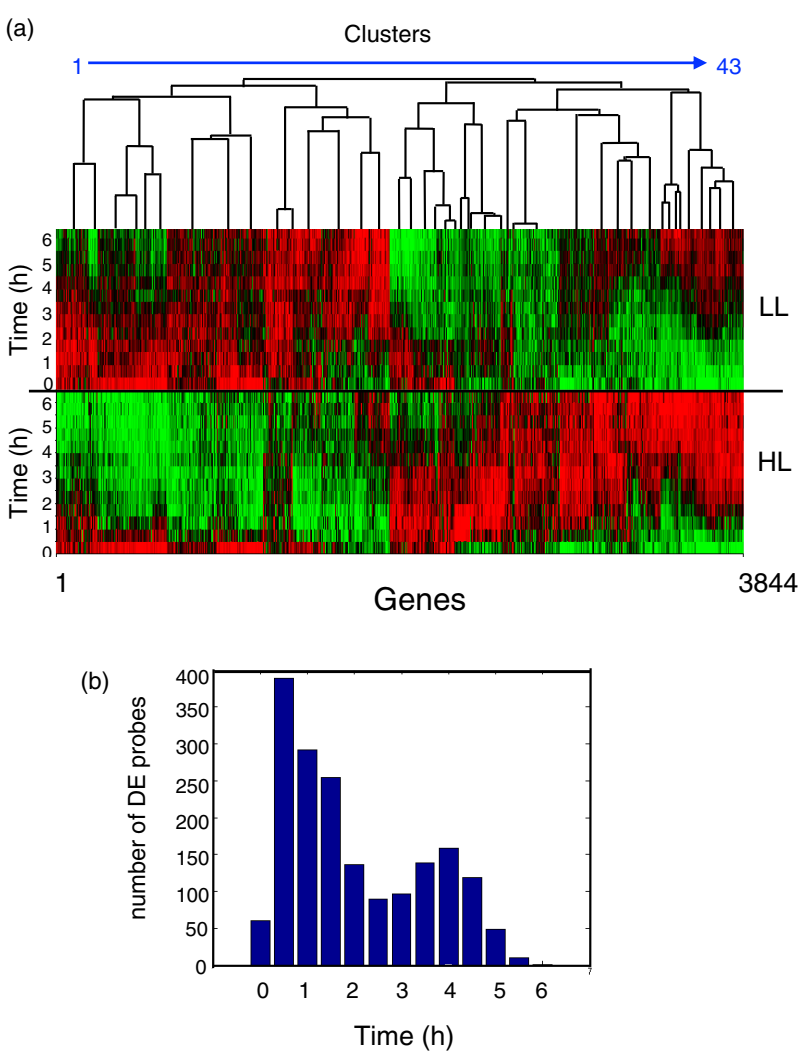

Figure 1. Temporal patterns of gene expression in LL- and HL-exposed leaf 7.
(a) Visual output of co-clustered expression values by SPLINECLUSTER. This was done for the 3844 genes already identified as differentially expressed in high light (HL) versus low light (LL) over the time of the experiment (see Results and Data S1). The values range from $\log_2$ 2.5 (red) to $-\log_2$ 2.0 (green). The 43 temporal clusters can be counted in the accompanying dendrogram. Time points are shown on the *y*-axes for the HL and LL gene expression.
(b) Number of HL/LL differentially expressed (DE) probes first appearing at each time point.

and/or display a downward pattern over the diel (Figure 1a; e.g. clusters 3 and 13 in Figure S1). This pattern changes progressively with increasing degree of expression being higher in HL than LL but against a descending diel pattern in clusters 14–20 (Figure 1a; e.g. cluster 18 in Figure S1), followed by transient but progressively increasingly greater differential transcript levels in HL samples compared with LL in clusters 21–26 (Figure 1a; e.g. cluster 23 in Figure S1) to progressively sustained periods of higher expression in HL compared with LL from clusters 27 to 43 against a background of level or increasing transcript levels across the diel (Figure 1a; e.g. clusters 33 and 43 in Figure S1).

To gain a better view of the timings of differential expression in response to HL, the DEGs from the time-local GP2S (Data S1) were used to identify intervals of differential expression as described by Windram et al. (2012). A histogram of the time of first differential expression (HL compared with LL) is shown in Figure 1(b) and indicated that the response to HL was rapid with >700 genes becoming differentially expressed by 1 h into the HL time course. Nevertheless, it was also clear that changes in transcript abundance were being initiated for significant numbers of genes up to 4 h HL. In summary, the response of the leaf 7 transcriptome to HL entails changed expression in response to the stimulus, with changes occurring across the time of the experiment against a backdrop of complex changes in transcript abundance across 6 h of an 8-h photoperiod.

Gene Ontology (GO) analysis showed that clusters 22, 23, and 25 were highly enriched for generic abiotic stress-defensive genes ($P \leq 0.1$, Bonferroni corrected; Data S2). In contrast, some of the other clusters displayed a different set of GO function enrichments (Data S2). These multiple enriched sets were consistent with a readjustment to cellular metabolism. For example, in clusters 39 and 41–43 with generally higher expression in HL compared with LL, there was over-representation of genes associated with amino acid and protein synthesis respectively. Among the clusters showing a lowered expression in HL compared with LL, there was enrichment for genes associated with cell wall metabolism (callose deposition, cell wall thickening cluster 1), phenylpropanoid and glucosinolate metabolism (clusters 1 and 10 respectively), basal resistance to infection (cluster 3), and chromatin re-modelling (cluster 10).

Assessing the effect of a temperature increase accompanying HL exposure

The HL exposure raised leaf temperature by 5°C within 5 min of exposure that remained at this level for the remainder of the experiment (Gorecka et al., 2014). To determine the effect of this raised temperature (and the accompanying change in vapour pressure deficit) on the wider leaf transcriptome, a microarray analysis was carried out on plants exposed to HL for 30 min, or 27°C under LL for 30 min (LL/27°C) compared with LL/22°C control plants. There were 609 DEGs [1.5-fold change; false discovery rate (FDR) <0.05] that responded to HL and/or LL/27°C (Data S3; see also GSE87755 and GSE87756). Of these DEGs, 73 responded to the temperature increase alone (Data S3) but were not removed from the time-series data.

Two recent transcriptomics studies in Arabidopsis were also relevant to assessing the impact of temperature rises on foliar HL responses (Balfagón et al., 2019; Huang et al., 2019). HL time-series DEGs in clusters 3–7, 9, 12, 14, 16, 30, 31, 36, and 39–43 (Figure 1a; Data S1) showed significant overlaps ($P < 0.00001$; Hypergeometric Distribution Test) with DEGs from Arabidopsis plants exposed to 7-h 600 μmol m^{-2} sec^{-1} HL (from a growth PPFD of 50 μmol m^{-2} sec^{-1}), which caused an increased leaf temperature of approximately 4°C (Data S4; Balfagón et al., 2019). In contrast, in the same study inclusion of a heat stress (42°C from growth at 23°C) as well as HL, substantially lowered the number and altered the pattern of overlap with the temporal clusters (Data S4; clusters 14–16, 19, 21, 22, 25, 26, 30, and 42). Elimination of a heat stress component in a HL experiment was achieved on 7-day-old seedlings exposed to 1200 μmol m^{-2} sec^{-1} (from a growth PPFD of 60 μmol m^{-2} sec^{-1}) for up to 72 h (Huang et al., 2019). In this study, ≤6 h HL exposure resulted in significant overlaps ($P < 0.00001$) with only four DEG clusters (4, 5, 9, and 19; Data S4). In contrast, using a pooled dataset of all HL DEGs throughout the 72-h experiment (Huang et al., 2019), 31 of 43 clusters displayed significant overlap with them (Data S4).

In conclusion, the elevated irradiance was the major environmental factor contributing to changes in transcript abundance. The 4–5°C temperature rise in fully expanded leaves accompanying the HL did not cause irreversible photoinhibition (Balfagón et al., 2019; Huang et al., 2019).

Induction of acclimation by repeated exposure to HL

To test our interpretation of the HL time-series data, we determined if HL acclimation could be induced by exposing a plant every day to 4 h HL (see Experimental procedures). This period of HL exposure was chosen as most differential expression had been initiated by this time (Figure 1b). Other than being shortened to 4 h, the environmental conditions were the same as for the time-series transcriptomics experiment (see Experimental procedures). The daily HL regime brought about a stepwise increase in the operating efficiency of PSII (Fq′/Fm′; Baker, 2008) of fully expanded leaves (Figure 2a; Data S5). By day 5, the PSII operating efficiency had increased substantially (e.g. 78% at 800 μmol m^{-2} sec^{-1} actinic PPFD; Figure 2b; see also Figure 4b). This pattern was followed by equivalent changes in Fv′/Fm′ and Fq′/Fv′ (Figure S2a; Data S5). Fv′/Fm′ indicates the maximum operating efficiency of PSII at

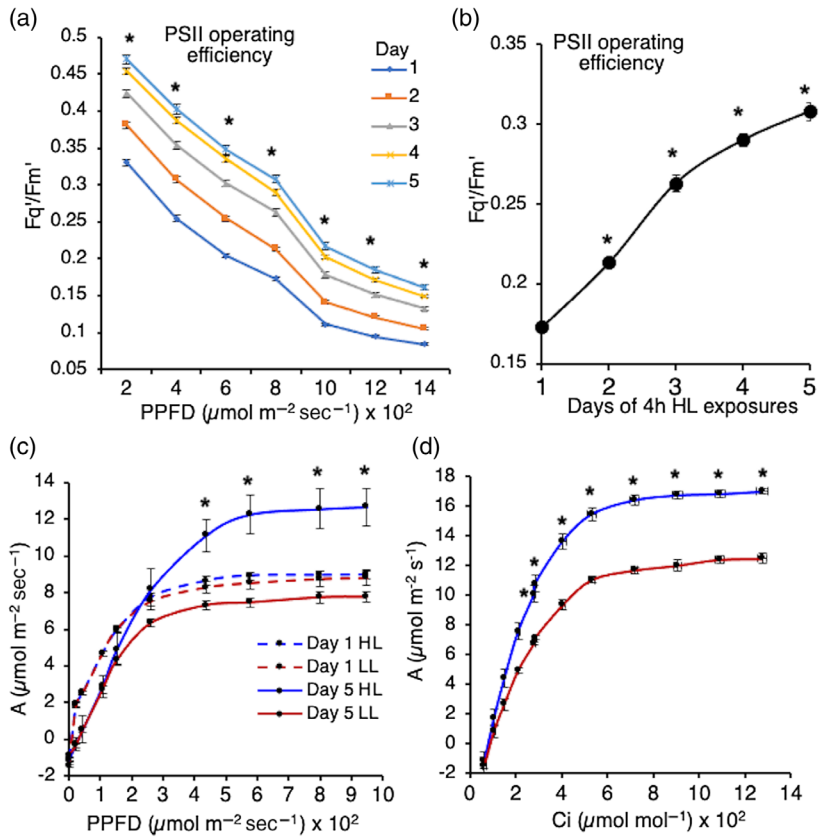

Figure 2. Induction of acclimation by repeated daily exposure to high light (HL).
(a) Plants were exposed daily to 4 h HL and Fq′/Fm′ determined for mature leaves. After the HL, plants were dark adapted and imaged under increasing actinic photosynthetically active photon flux densities (PPFDs) from 200 to 1400 μmol m^{-2} sec^{-1} in 200 μmol m^{-2} sec^{-1} increments every 5 min. Data were collected as chlorophyll fluorescence images and processed digitally to collect values from mature leaves. Plants were treated in this way daily for 5 days: day 1 (blue), day 2 (red), day 3 (olive green), day 4 (purple), and day 5 (light blue). Data (mean ± SE) correspond to 38 plants at 24–28 days post-germination (dpg) over six experiments, and the asterisks show differences in chlorophyll fluorescence parameters between days 1 and 5 were significant ($P \leq 0.001$; ANOVA and Tukey HSD). Full statistical data comparing all days of HL exposure are provided in Data S5.
(b) Daily changes in Fq′/Fm′ plotted from the data in A and Data S5 (right panel). Fq′/Fm′ values are from the same plants over the daily HL exposures showing the increase in photosystem II (PSII) operating efficiency at 800 μmol m^{-2} sec^{-1} PPFD actinic light over the 5 days of the experiments.
(c) Photosynthesis plotted as CO_2 assimilation rate (A) as a function of actinic PPFD in mature leaf 7 (mean ± SE; $n = 8$ plants for each treatment; 49 dpg). Measurements were taken the day after 1 (dashed lines) and 5 days (solid lines) of daily 4 h HL exposures (blue lines) along with the low light (LL) control plants (red lines) not subjected to this treatment.
(d) Photosynthesis plotted as CO_2 assimilation rate (A) as function of leaf internal CO_2 concentration (C_i) in mature leaf 7 (mean ± SE; $n = 8$ plants for each treatment; 49 dpg). Measurements were taken the day after 5 days of daily 4 h HL exposures (blue line) along with the LL control (red line). A was determined by infra-red gas analysis (see Experimental procedures). Asterisks indicate significant differences ($P < 0.02$; covariant T and two-tailed F tests) between LL- and HL-exposed plants.

a given PPFD and a rise in this parameter indicates a decline in NPQ (Baker, 2008). Fq′/Fv′ is the PSII efficiency factor and it is mathematically identical to the coefficient for PQ (q_p) and indicates increased capacity to drive electron transport (Baker, 2008). LL-grown plants of the same age as the plants subjected to five daily HL treatments did not show these changes in chlorophyll fluorescence (CF) parameters (Figure S2b; Data S5).

The first exposure to HL (day 1) did not result in irreversible photoinhibition (Figure S3a) or significant tissue damage (Figure S3b). This was confirmed in the HL time-series data, which used the same PPFDs, in which steady levels of transcripts for genes considered to be markers for H_2O_2 (*APX2* and *FER1*; Ball et al., 2004; Gadjev et al., 2006) rose but those associated with $^1O_2$-induced signalling (*AAA-ATPase* and *BAP1*; Ramel et al., 2013) remained unchanged or declined (Figure S3c). The changes in expression of these marker genes indicated the HL treatment used in the time-series transcriptomics experiments, also did not elicit photodamage and provided conditions that could promote HL acclimation.

The increased operating efficiency of PSII (Fq′/Fm′ and Fq′/Fv′) after the 5-day HL treatment (Figure 2a; Figure S2a; Data S5) could have reflected enhanced photosynthetic capacity. To test this possibility, gas-exchange measurements for photosynthesis were carried out (see

Experimental procedures). The same experiment was repeated and, in the photoperiod following the last HL treatment, measurements were taken of CO_2 assimilation rates (A) over a range of light intensities in fully expanded leaf 7 of these plants (Bechtold et al., 2016). This showed that the light-saturated photosynthetic rate (A_{sat}) was significantly greater ($P < 0.001$) by 64% compared with the LL control plants (Figure 2c). In contrast, after a single 4 h HL exposure, followed by photosynthesis measurements in the next photoperiod, no increase in A_{sat} was observed (Figure 2c). In a separate series of experiments, the measurement of A over a range of internal leaf CO_2 concentrations (Ci) also showed that the maximal CO_2-saturated rate of photosynthesis (A_{max}) increased by 31% ($P < 0.002$) after five daily HL exposures (Figure 2d). This confirmed that repeated HL exposures did not solely affect stomatal behaviour but brought about an increase in foliar photosynthetic capacity. The changes in CF parameters by day 5 of HL treatments observed in the previous experiments (Figure 2a) occurred also in larger older leaves that were required for gas exchange measurements (Figure S2c; see Experimental procedures).

In summary, increased A_{sat} and A_{max} after 5 days of repeated HL exposure (Figure 2c,d) was accompanied by a highly significant increase in Fq′/Fm′ (Figure 2a; Figure S2c; $P < 0.0001$, ANOVA and Tukey HSD; Data S5). Therefore, a substantial (>40%; typically using the median 800 μmol m^{-2} sec^{-1} actinic PPFD value) change in Fq′/Fm′ between days 1 and 5 of repeated HL was subsequently used as a more convenient image-based measurement of the establishment of increased photosynthetic capacity, which was taken as indicative of HL acclimation.

Dynamic statistical modelling infers a BBX32-centric HL gene regulatory network

The HL time-series data were used to infer gene regulatory networks (GRNs) using VBSSM (Beal et al., 2005; Penfold and Wild, 2011). We chose VBSSM because it has been demonstrated to infer known GRNs from temporal gene expression data and to infer novel GRNs whose highly connected genes (nodes) have subsequently been shown experimentally to have a novel and important function (Beal et al., 2005; Bechtold et al., 2016; Breeze et al., 2011; Penfold and Buchanan-Wollaston, 2014; Penfold and Wild, 2011; Windram and Denby, 2015). However, due to the limited number of time points, we opted to infer networks for about 100 genes or probes to avoid overfitting by constraining network size (Allahverdiyeva et al., 2015; Beal et al., 2005; Bechtold et al., 2016; Windram and Denby, 2015). To accommodate this limitation, we focused on DEG coding for transcription regulatory genes such as transcription (co-)factors (TFs). We reasoned that regulatory networks composed of such genes would control the expression of a wide network of genes and by inferring GRNs this would allow us to identify and focus on the most connected of them, often termed hub genes (Albihlal et al., 2018; Windram and Denby, 2015). Consequently, we reasoned that such regulatory genes would control the expression, directly and indirectly, of a sufficiently large number of genes to influence whole leaf HL responses and acclimation phenotypes. Therefore, the intention was to screen highly connected candidate regulatory hub genes directly for their impact upon HL acclimation measured as changes in photosynthetic efficiency.

It was estimated that there were 371 HL DEGs coding for TFs or (co-)TFs (Data S6). To narrow our selection further, comparisons were made between the 43 HL temporal clusters (Figure 1a; Data S1) and 14 publicly available transcriptomics datasets or meta-analyses of such data for HL treatments or mutants perturbed in chloroplast-to-nucleus and reactive oxygen species-mediated signalling (Data S4). On a cluster-by-cluster basis, the highest number of significant ($P < 0.00001$) overlaps in clusters 1, 2, 3, 5, 6, 9, 10, 14, 16, 17, and 27 were encountered with *phyA/phyB* DEGs (Data S4; Shikata et al., 2014). This observation suggested that photoreceptor-mediated regulation of HL-responsive genes was highly represented in the time-series transcriptomics dataset. Therefore, we examined whether photoreceptor-regulated (co-)TF genes (Dong et al., 2014; Shikata et al., 2014) were also over-represented in the HL dataset. This was the case with 91 photoreceptor- and light-regulated (co-)TF DEGs identified irrespective of which temporal cluster they were drawn from ($P = 1.4E-06$; Hypergeometric Distribution Test, Data S6). The HL time-series expression data from these 91 genes were used to infer networks with VBSSM.

The first inferred network for HL revealed *LATE ELONGATED HYPOCOTYL* (*LHY*) as the most highly connected gene (Figure S4a). However, mutant *lhy-21* plants were not perturbed in HL acclimation (Figure S4b). Therefore, the VBSSM modelling was reiterated but omitted the *LHY* expression data. This inferred a 47 node-HL network centred on *BBX32* (Figure 3). The transcript levels of the 12 most connected nodes (≥3 edges) across the time series, under LL and HL conditions, is shown in Figure S5 and shows the diversity of expression patterns derived from the temporal clusters (Data S1; Figure 1a,b).

BBX32 is a negative regulator of photosynthetic capacity and HL acclimation

Acclimation was tested in two independent *BBX32* overexpressing (*BBX32*-OE) genotypes (BBX32-10 and BBX32-12) and a T-DNA insertion mutant (*bbx32-1*; see Experimental procedures and Holtan et al., 2011). *BBX32*-OE plants showed some inhibition of Fq′/Fm′ after day 1 of HL (Data S7) but a highly significant impairment of the increase in PSII operating efficiency at the end of the 5-day serial HL exposure indicative of an inhibition of HL acclimation

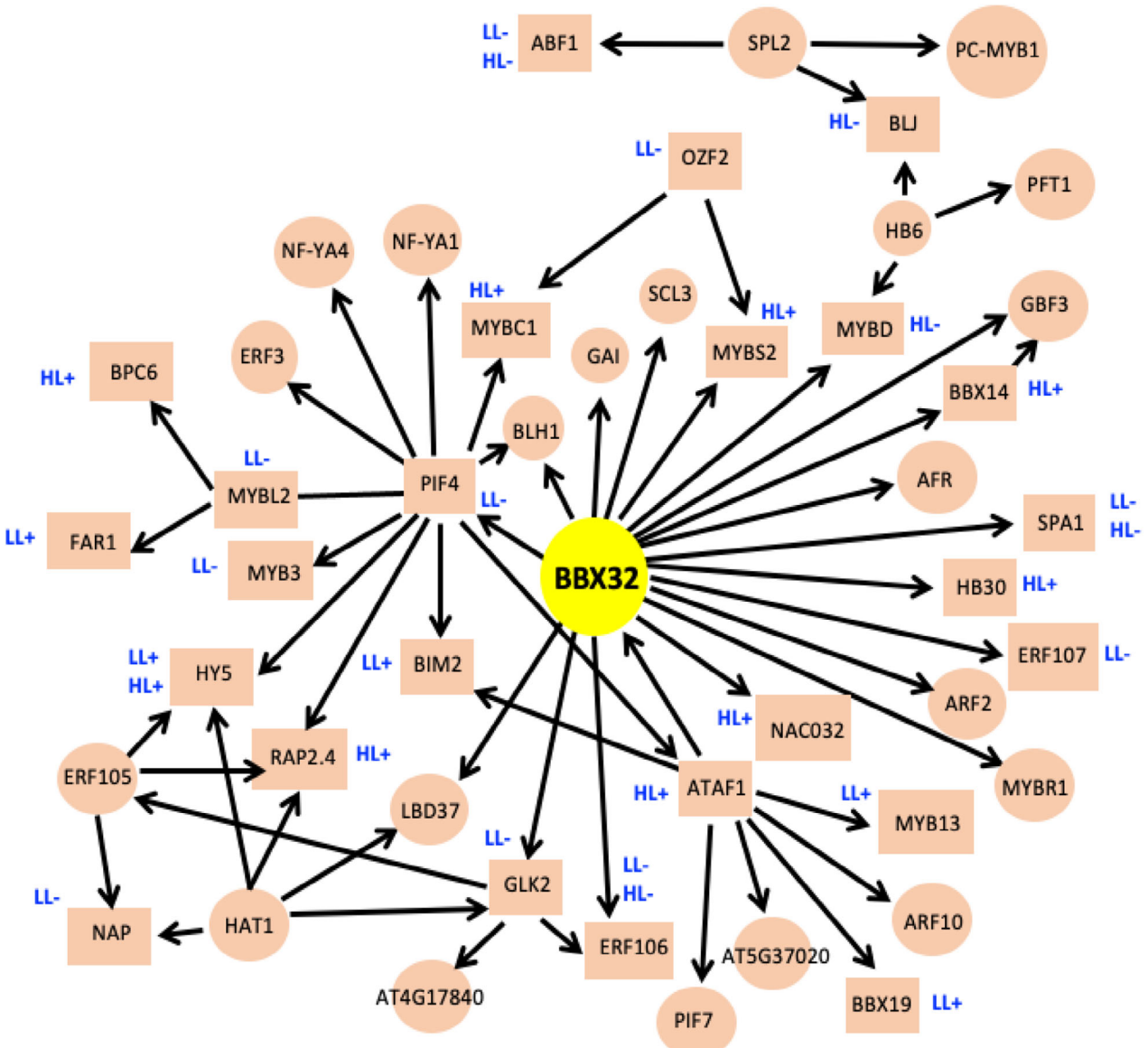

Figure 3. Inferred high light (HL) gene regulatory network centred on *BBX32*.
The network shown was generated from the time-series expression data for HL differentially expressed genes. Differentially expressed genes code for transcription (co-)factors that are also light- and/or *PHYA/PHYB*-regulated in de-etiolating seedlings. The network was generated using VBSSM (threshold *z*-score = 2.33; see Experimental procedures) and initially visualized using CYTOSCAPE (v3.3.2; Shannon et al., 2003) but redrawn manually to improve clarity. The network shown is from the second iteration of the modelling, which omitted expression data for *LHY* (First iteration; Figure S4a). Genes depicted in rectangular nodes were responsive to *BBX32* overexpression in HL- and/or low light (LL)-exposed leaves by showing significantly ($P_{adj} < 0.05$; negative binomial distribution probability model and Benjamini–Hochberg correction) higher (+) or lower (+) transcript abundance than Col-0 (see Figure 5; Data S8). Locus codes for the network genes can be found in Experimental procedures.

(Figure 4a; Data S7). In contrast, *bbx32-1* plants showed a weak but significant accelerated acclimation phenotype (Figure 4b; Data S7). We define an accelerated acclimation phenotype as a significant enhancement of PSII operating efficiency over one or more days in the 5-day serial HL treatment. The strong negative impact of *BBX32* overexpression on acclimation was confirmed subsequently by showing a significant inhibition of photosynthetic capacity (A_{sat}) after the 5 days of daily 4 h HL (Figure 4c).

Transcriptomics provides a partial verification of the BBX32 HL TF network

To explore further the connections depicted in the network model (Figure 3), massively parallel RNA sequencing (RNA-seq) was carried out (see Experimental procedures; GEO; GSE158898) to profile the foliar transcriptome of fully expanded leaves of Col-0 and *BBX32*-OE plants exposed to 3.5-h HL in comparison with LL controls. From these data,

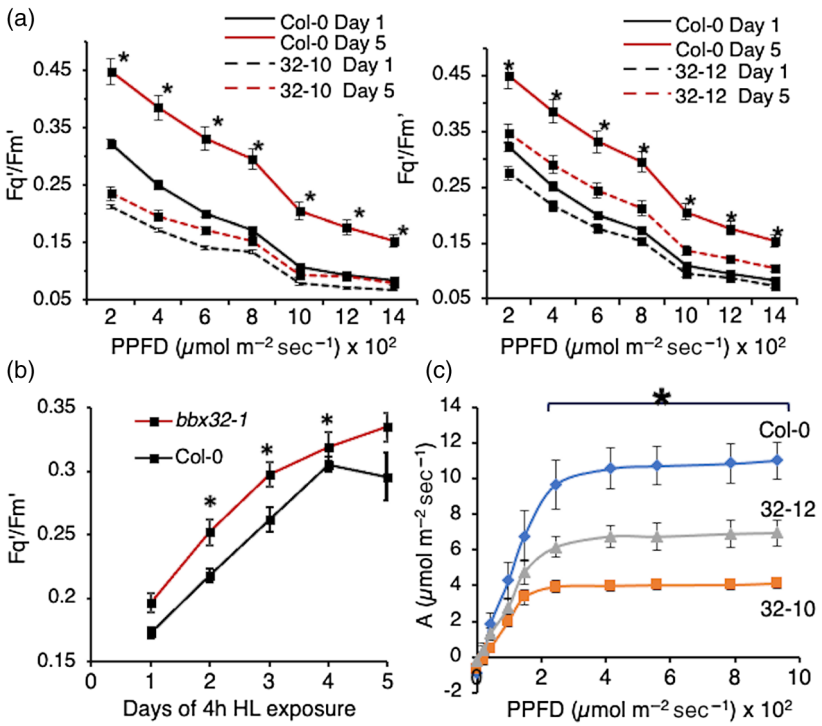

Figure 4. Acclimation in *BBX32* overexpression and *bbx32-1* plants.
Fq′/Fm′ values determined from images of ≥4 mature leaves from eight plants (24–28 days post-germination) over two experiments (means ± SE), which had first been exposed to 4 h high light (HL) each day for 5 consecutive days (see Experimental procedures and legend for Figure 2). Chlorophyll fluorescence parameter values were collected at a range of actinic photosynthetically active photon flux densities (PPFDs) (as indicated) at the end of each daily HL exposure.
(a) Fq′/Fm′ values at day 1 (black lines) and day 5 (red lines) for mutant or overexpression plants (dashed line) and Col-0 (solid line) of the HL treatments for BBX32-10 and BBX32-12. Asterisks indicate difference between mutant genotype and Col-0 at day 5 ($P < 0.01$; ANOVA and Tukey HSD).
(b) Daily Fq′/Fm′ values at 800 μmol m^{-2} sec^{-1} PPFD actinic light of *bbx32-1* compared with Col-0 showing differences that were significant ($P < 0.01$) only between days 2 and 4.
(c) Photosynthesis plotted as CO_2 assimilation rate (*A*) as a function of incident PPFD in mature leaf 7 of low light-grown BBX32-10 (green line) and BBX32-12 (red line) compared with Col-0 (blue line) plants after 5 days of daily 4 h HL (see Experimental procedures). Data are the mean ± SE; $n = 4$ for each genotype at 49 days post-germination; Asterisk indicates significant differences ($P < 0.02$; covariant *T* and two-tailed *F* tests) between Col-0 and BBX32-10 and BBX32-12 at a given PPFD. Leaf *A*, as a function of PPFD, was determined by infra-red gas analysis (see Experimental procedures).

the transcript levels of 25 of 47 constituent genes in the inferred network were significantly altered by constitutive *BBX32* overexpression compared with Col-0 plants in LL and/or HL (Figure 5; Data S8), partly validating the GRN.

Transcriptome of BBX32OE plants links initial responses to HL with dynamic acclimation

The impaired ability of *BBX32*-OE plants to photosynthesize (Figure 4a,c; Data S7) prompted an analysis of the RNA-seq data on the impact of *BBX32* overexpression on the transcript levels of photosynthesis-associated genes (PhAGs). There was a clear influence of *BBX32* overexpression under LL and HL on the transcript levels of a range of transcripts coding for LH Antenna proteins, Calvin–Benson cycle enzymes, and components of photosynthetic electron transport, PSI and PSII (Figure 6a; Data S8). We concluded that these and other transcripts affected in *BBX32*-OE plants might reflect their perturbed photosynthetic physiology. The establishment of dynamic acclimation (see Introduction) requires the expression of *GLUCOSE-6-PHOSPHATE/PHOSPHATE TRANSLOCATOR2* (*GPT2*; see Discussion; Athanasiou et al., 2010). HL differential *GPT2* transcript levels were evident (Figure 6b,c) placing it in temporal cluster 30 (Data S1). In addition, this change in *GPT2* transcript levels was strongly inhibited in *BBX32*-OE plants exposed to 3.5-h HL (Figure 6c).

This disruption of PhAG transcript levels led us to examine the impact of *BBX32* overexpression on other cellular processes. Of the 2903 genes whose transcript levels were HL responsive ($P < 0.05$; ≥ 2-fold differentially expressed; Data S9), *BBX32* overexpression perturbed the transcript levels of 32% and 15% of them in LL and HL conditions respectively (Figure 7a; Data S9). The HL/LL Col-0 DEGs were enriched for 35 GO BP terms and 26 of them were significantly over-represented in the *BBX32*-OE/Col-0 LL and *BBX32*-OE/Col-0 HL DEGs (Data S10). These shared GO groups all describe responses to various abiotic and biotic stresses or response to endogenous stimuli such as

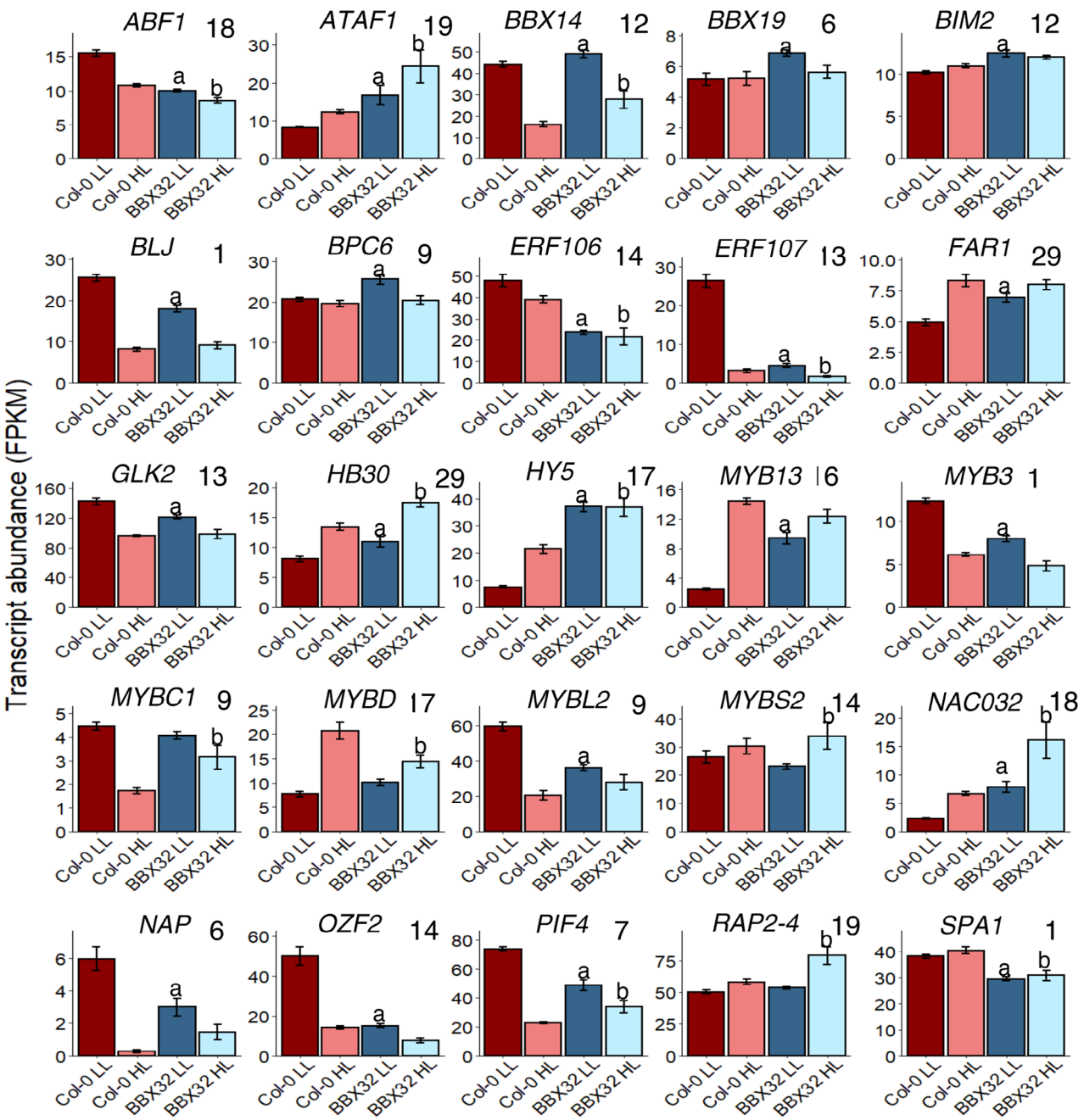

Figure 5. Partial validation of the *BBX32*-centric inferred gene regulatory network.
Expression of 25 of the 47 transcription factor genes in the inferred network showing the effect of *BBX32* overexpression. All the genes displayed significant differences ($P_{adj} < 0.05$; negative binomial distribution probability model and Benjamini–Hochberg corrected) in transcript abundance in four replicate *BBX32* overexpression plants compared with four Col-0 both under low light (LL; suffix 'a') and/or high light (HL; suffix 'b') conditions. Data are mean FPKM ($n = 4 \pm$ SE) from four plants per genotype and treatment. Tabulated FPKM data for these genes can be found in Data S8. Colour codes are brown and dark blue for Col-0 and *BBX32*-10 plants in LL respectively, salmon pink and light blue are Col-0 and BBX32-10 plants in HL. Cluster number for each gene is shown on each graph.

salicylic acid or H_2O_2. This analysis indicates that *BBX32* influences a wide range of cellular responses to stress, which includes regulation of genes associated with basal immunity to infection.

The DEGs from *BBX32*-OE HL- and LL-treated plants were also compared with the 3844 time-series HL DEGs (Figure 7b; Data S1 and S11). Although the number of overlapping genes was lower (Figure 7b), 256 *BBX32*-OE HL DEGs again confirmed enrichment for a range of GO terms that describe generic responses to environmental stress (Figure 7c; Data S11). However, the 408 *BBX32*-OE LL DEGs also differentially expressed in the HL time-series

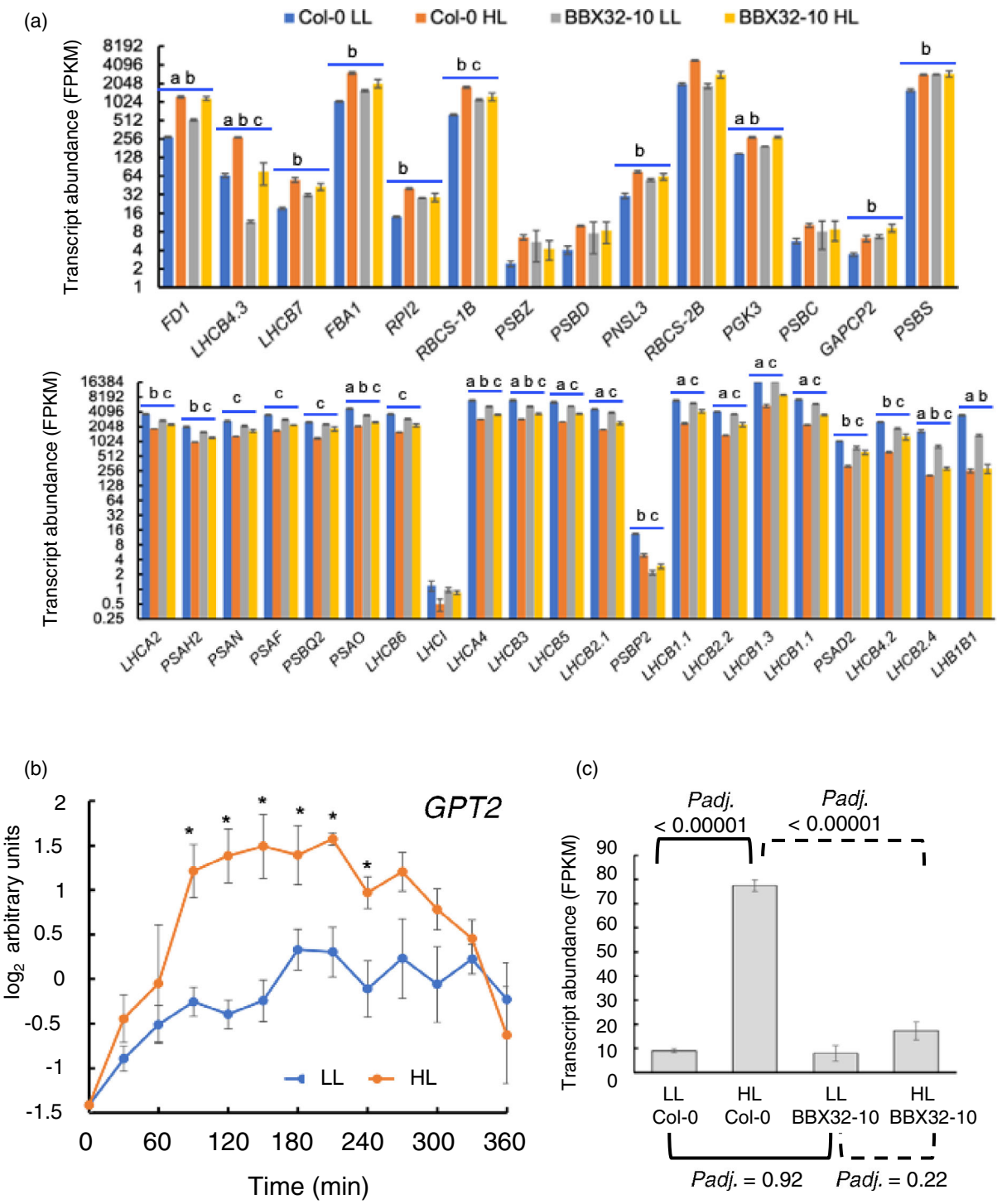

Figure 6. Transcript levels of photosynthesis-associated genes in *BBX32*-OE plants are perturbed.

(a) Transcript abundance as FPKM values from the fully expanded leaves of 4 Col-0 or BBX32-10 plants exposed to 3.5 h high light (HL) or low light (LL) control. Data are means ± SE (n = 4). Photosynthesis-associated genes are those defined on the KEGG database (https://www.kegg.jp/dbget-bin/www_bget?pathway+ath00195). Transcripts of photosynthesis-associated genes shown are those that displayed a >1.8-fold greater or a >2-fold lesser abundance in Col-0 HL compared with Col-0 LL (P_{adj} < 0.05; P value from negative binomial distribution model; Benjamini–Hochberg corrected). Suffixes 'a'–'c' refer to P_{adj} < 0.05 for: 'a' BBX32-10 HL/BBX32-10 LL; 'b' BBX32-10 LL/Col-0 LL; 'c' BBX32-10 HL/Col-0 HL. These data are in Data S8.

(b) Expression of *GPT2* in 0–6 h HL and LL. Log_2-transformed fluorescence values (mean ± SE; n = 4) were normalized with respect to the same values at the zero-time point and are shown for the HL (red line) and LL (black line) data. Asterisks denote significant difference between LL and HL ($P \leq 0.05$; ANOVA; Data S1) at each time point.

(c) *GPT2* expression in BBX32-10 and Col-0 plants (n = 4 ± SE; P_{adj} as in a) exposed to HL and LL.

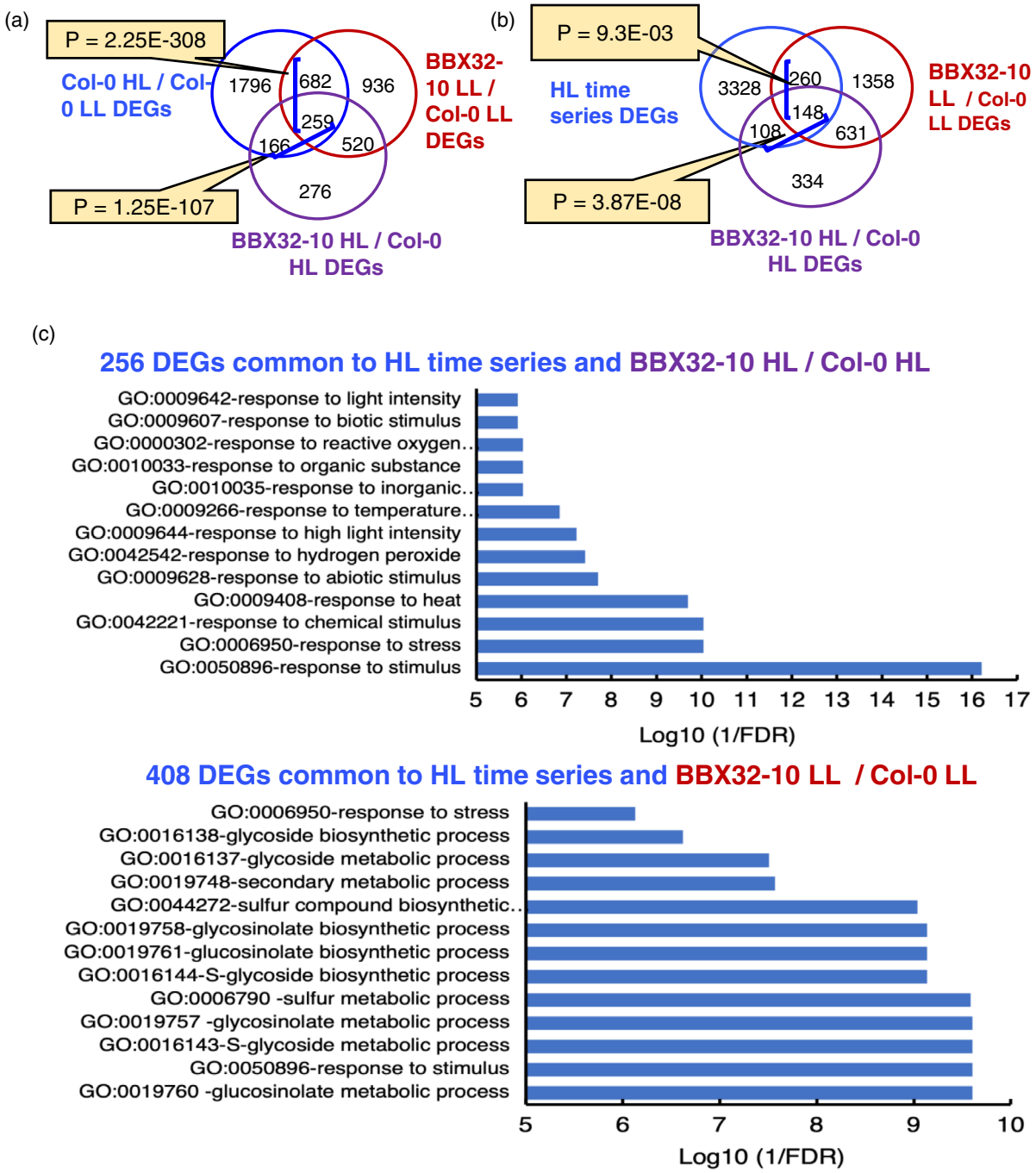

Figure 7. Comparisons of genes affected by *BBX32* overexpression (OE) with high light (HL) differentially expressed genes (DEGs) in Col-0.
(a) Venn diagram of overlapping DEGs between Col-0 and *BBX32*-OE plants under low light (LL) and HL conditions compared with DEGs responsive in Col-0 to 3.5 h HL and generated by RNA-sequencing. Relevant three groups of DEGs can be found in Data S9.
(b) Venn diagram as in (a) except the *BBX32*-OE DEGs were compared with the 3844 time-series HL DEGs in Data S1, which were derived from microarray-based transcriptomics data (see Results and Experimental procedures). DEGs in the overlapping segments are listed in Data S10.
(c) Top enriched Biological Process GO Terms from genes shared between the 3844 HL time-series DEGs and the 256 BBX32-OE HL/Col-0 HL DEGs (top panel) and 408 BBX32-OE LL/Col-0 LL DEGs (bottom panel) respectively. FDR, false discovery rate.

dataset, also revealed significant enrichment (FDR <0.05) of a range of additional functions (Figure 7c; Data S11) including glucosinolate and glycosinolate metabolism (GO:0019760, GO:0050896, GO:006143, GO:0019757, GO:0016144, GO:0019761, GO:0019758), cell wall thickening (GO:0052543, GO:0052386), and callose deposition (GO:0052543, GO:0052545). Downregulation of these groups of genes in the HL time-series data (Data S1 and S2) may reflect a redistribution of resources towards HL acclimation and away from basal immunity (see above and Discussion). The observations also reinforce that *BBX32* influences immediate responses before or during a single exposure to HL.

CRY1 and *HY5* control of photosynthetic efficiency and acclimation

BBX32 has been proposed to be a negative regulator of the integration of light signals from phytochromes (PHYs) and cryptochromes (CRYs) during photomorphogenesis (Gangappa and Botto, 2014; Holtan et al., 2011). *BBX32*-OE seedlings display long hypocotyls in the light phenocopying photoreceptor mutants and mutations in *LONG HYPOCOTYL5* (*HY5*; Holtan et al., 2011). Notably, *HY5* is a member of the *BBX32*-centric GRN (Figures 3 and 5) and along with *CRY1*, has also been implicated in influencing the expression of HL-inducible gene expression (Chen et al., 2013; Kleine et al., 2007; Shaikhali et al., 2012). Furthermore, *PHYA*-, *PHYB*-, and *CRY1*-mediated signalling was proposed to regulate photosynthetic capacity in plants grown in a range of PPFDs (Walters et al., 1999; see Introduction). These considerations prompted us to test HL acclimation in photoreceptor-defective and *hy5* mutants.

No significant impact of *PHYA* or *PHYB* on acclimation was observed (Figure S6a,b). In contrast, *cry1* mutants almost completely failed to undergo any acclimation (Figure 8a,b), whereas *cry2-1* was not impaired (Figure S6c). One of the *cry1* mutants shown (*cry1*-M32; Figure 8b) arose serendipitously from a screening of T-DNA insertion mutants in genes coding for 7-transmembrane proteins that had been postulated to be implicated in HL-mediated G protein signalling (Galvez-Valdivieso et al., 2009; Gorecka et al., 2014). However, the one mutant recovered from this screening, was shown subsequently to be deficient in HL acclimation due to a disabling second site mutation in *CRY1* (see Experimental procedures). As the defective acclimation phenotype was identified before knowing the identity of the causal mutation, we took this to be forward genetic evidence of the importance of *CRY1* in setting PSII operating efficiency in mature leaves.

The light environment used to grow plants for this study and subject to HL was enriched for blue wavelengths (Figure S7; see Discussion). Therefore, we considered the possibility that a role for PHYs in dynamic acclimation could be obscured, favouring a predominance of CRY1 under our growth conditions. To test this notion, a mutant harbouring a constitutively active form of PHYB, phyBY276H (*YHB*) in a Col-0 background (Jones et al., 2015) was tested for HL acclimation (Figure 8c). This mutant exhibited a higher PSII operating efficiency than Col-0 after 1 day of HL exposure consistent with an accelerated acclimation phenotype.

Mutants defective in *HY5* function were strongly impaired in HL acclimation (Figure 8d,e) consistent with being a member both of a *BBX32*-centric GRN (Figures 3 and 5, Data S8).

COP1, PIF, and SPA genes regulate photosynthetic efficiency and HL acclimation

In both photomorphogenesis and shade avoidance responses, the transduction of signals from photoreceptors is mediated via one or more DET/COP/FUS regulatory complexes (Lau and Deng, 2012), which act as platforms for the post-translational control of the levels of HY5 and the integration into the signalling of TFs, PHYTOCHROME INTERACTING FACTORS (PIFs), and regulatory proteins, SUPPRESSOR OF PHYA-105 (SPA) (Dong et al., 2014; Gangappa and Botto, 2016; Hardtke et al., 2000; Hoecker, 2017; Huang et al., 2014; Lau and Deng, 2012; Lau et al., 2019; Lian et al., 2011; Pham et al., 2018; Toledo-Ortiz et al., 2003). In the VBSSM-inferred GRN, *PIF4*, *PIF7*, and *SPA1* were predicted to have a regulatory connection to *BBX32* (Figures 3 and 5).

Cop1-4 plants, despite a severely dwarfed shoot morphology (Figure 9a; Deng and Quail, 1992; Gangappa and Kumar, 2018), displayed an accelerated acclimation phenotype (Figure 9b) such as the HL response of *YHB* plants (Figure 8c). In contrast, despite a similar dwarf shoot morphology (Figure 9a), *det1-1* displayed no defect in HL acclimation (Figure 9d). This suggests that the HL acclimation response of chloroplasts is independent of shoot size and that these two traits are not coupled. Furthermore, *spa1/spa2/spa3 (spa1,2,3)* plants also displayed accelerated HL acclimation (Figure 9c). Therefore, it was concluded that one or more type of the COP1/SPA complex (Hoecker, 2017; Huang et al., 2014) are negative regulators of HL acclimation and that *DET1* plays no role in this process.

There is a high degree of redundancy among the *PIF* family and therefore a quadruple null mutant of *PIF1*, *3*, *4*, and *5* (hereafter called *pifq*; Leivar et al., 2008) was tested and shown to display significant inhibition of HL acclimation (Figure 9e). In contrast, the HL acclimation of a single mutant allele of *PIF4* (*pif4-2*) was normal (Figure S6d).

DISCUSSION

Time-series HL transcriptomics data indicate the initiation of acclimation processes

The exposure to a 7.5-fold increase in PPFD (HL) presents both a threat and an opportunity to the plants in this study.

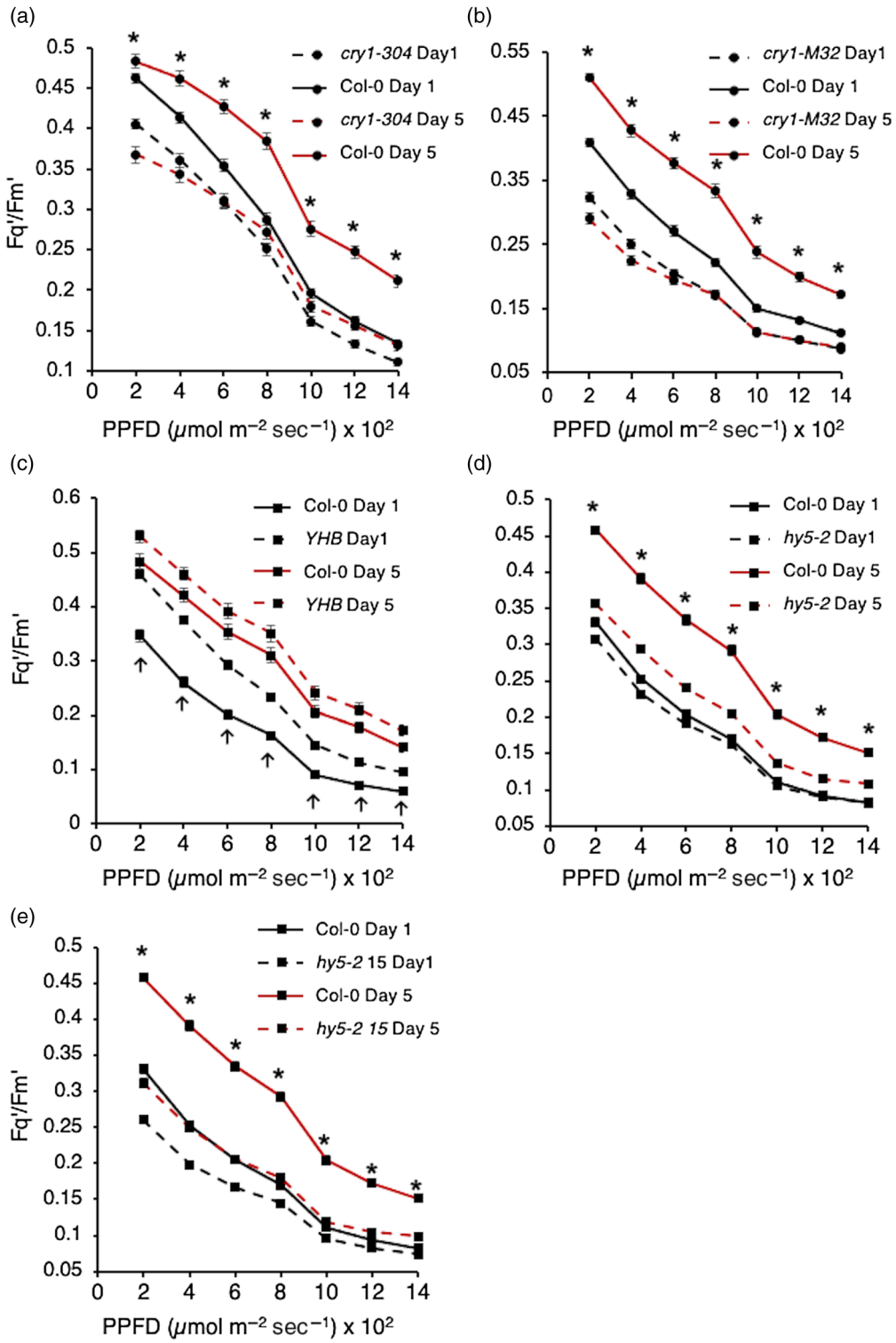

Figure 8. High light (HL) acclimation of photoreceptor and *HY5* mutants.
Plots show the photosystem II operating efficiencies (Fq′/Fm′) determined from chlorophyll fluorescence images of ≥4 mature leaves from eight plants over two experiments (means ± SE). Plants had been exposed to 4 h HL each day for 5 consecutive days (see Experimental procedures and legend of Figure 2). Chlorophyll fluorescence parameter values were collected at a range of actinic photosynthetically active photon flux densities (PPFDs) at the end of days 1 and 5 of HL. Fq′/Fm′ values at day 1 (black lines) and day 5 (red lines) for mutant plants (dashed line) and Col-0 (solid line) of the HL treatments for (a) *cry1-304*, (b) *cry1-M32*, (c) *YHB*, (d) *hy5-2*, and (e) *hy5-215*. Asterisks (panels a, b, d, e) indicate significant difference between mutant compared with Col-0 at day 5 ($P < 0.01$; ANOVA and Tukey HSD). Upward arrows (c) indicate significant difference between YHB and Col-0 at day 1 ($P < 0.01$; ANOVA and Tukey HSD).

The threat comes from the possibility that the PPFD will continue to increase and render the plant susceptible to irreversible photoinhibition. The opportunity comes from enhancing photosynthetic capacity and consequently acclimating to the HL (Figure 2a–d), accompanied by a lowered reliance on the dissipation of excitation energy using NPQ (Figure S2a), which can limit plant productivity (Kromdiijk et al., 2016).

The adaptation to a potential increase in photo-oxidative stress and photoinhibition (see Introduction) is the early (≤ 1 h), strong, but transient change in transcript abundance of 257 genes in clusters 21–26, upon exposure to HL. Clusters 22, 23, 25, and 26 include among them 64 known genes that promote abiotic stress tolerance (Figure 1a,b; cluster 23 in Figure S1; Figure S2c; Data S1 and S2). The transiently enhanced expression of these genes presumably allows the plant to overcome any potential initial detrimental effects of the HL exposure, as many other studies have reported (e.g. Balfagón et al., 2019; Ball et al., 2004; Crisp et al., 2017; Gadjev et al., 2006; Huang et al., 2019; Ramel et al., 2012, 2013; Willems et al., 2016).

Coordinated alteration in specific biological processes was evident in some clusters. Downregulated clusters include those collectively associated with aspects of basal or innate resistance to pathogens (Piasecka et al., 2015; Underwood, 2012). Examples include genes coding for cell wall modifications and callose deposition (cluster 1), defence response to bacteria (cluster 3), and glucosinolate/glycosinolate biosynthesis (cluster 10). In this study, plants were grown at a PPFD below their light saturated rate of photosynthesis (A_{sat}; Figure 2c; see Experimental procedures). Plants grown under such light-limiting conditions may initially reallocate resources away from some cellular processes to begin acclimation and take advantage of a sustained increase in PPFD. Photosynthetically active expanded but not senescing leaves, such as leaf 7 used here (Bechtold et al., 2016), may maintain a higher degree of poising of immunity to respond to biotic stress compared with abiotic stress (Berens et al., 2019). Therefore, in a converse situation where a potential abiotic stress threat emerges, the diversion of resources from defence against pathogens may be an appropriate response. Meanwhile, among the DEG time-series clusters whose transcript levels increased at various points in the experiment, are those that could be preparing the leaf to increase its photosynthetic and metabolic capacity to begin acclimation (Dietz, 2015 ; Eberhard et al., 2008). Genes in over-represented GO BP terms included those involved in macromolecule synthesis and particularly translation (clusters 41–43) and related metabolic processes such as enhanced amino acid and organic acid biosynthesis (cluster 39). The HL induction of transcript levels of one gene, *GPT2*, in temporal cluster 30 (Data S1), is noteworthy (Figure 5b). This gene is required for dynamic acclimation (Athanasiou et al., 2010) and this change in expression may indicate initiation of HL acclimation processes.

BBX32 connects a range of cellular processes during the response to HL

Of all the comparisons carried out with relevant transcriptomics datasets, the most extensive overlap with time-series HL DEGs was with those from dark-germinated *phyA/phyB* seedlings exposed to red light (Data S4; Shikata et al., 2014). While this was initially surprising because of the very different experimental conditions, earlier studies had shown a strong influence of photoreceptor genes (*CRY*s and *PHY*s) on photosynthetic capacity in Arabidopsis grown at a range of PPFDs (Walters et al., 1999) and photoreceptor-directed signalling on the induction of HL-responsive genes (Guo et al., 2016; Huang et al., 2019; Kleine et al., 2007; Shaikhali et al., 2012).

The above analysis prompted a selection of 91 light- and PHYA/B-regulated (co-)TF genes (Data S6). The HL time-series expression data from these genes were subjected to VBSSM, which after two iterations, inferred a highly interconnected *BBX32*-centric (co-)TF GRN (Figure 3; Figure S4; see Results). In the GRN, >50% of the nodes (genes) were subsequently confirmed by RNA-seq to be influenced significantly in their expression by *BBX32* (Figures 3 and 5; Data S8).

BBX32 showed a greater transcript abundance over LL controls at any point onwards from 2 h HL. Nevertheless, its transcript abundance was on a downward trend through the diel, paralleling its LL pattern of expression (Figure S5). Interestingly, while *BBX32*-OE plants displayed a 66-fold elevated *BBX32* transcript level in LL, this reduced to 33-fold after 3.5 h HL (Data S9). The enhanced *BBX32* expression in these plants is driven by the CaMV 35S promoter (Holtan et al., 2011); therefore, the decline in transcript abundance over a diel could indicate that a temporal post-transcriptional control operates on *BBX32* expression.

The overexpression of *BBX32* strongly influenced the immediate responses of plants to HL across a range of cellular processes (Figure 6c; Data S8 and S9) and in their photosynthetic physiology (Figure 4a–d). Most prominently, under LL, *BBX32*-OE plants displayed perturbed expression of genes with basal immunity, including multiple GO designations for glucosinolate/glycosinolate metabolism, callose deposition, and responses to chitin and to pathogens (Figure 7c; Data S10 and S11). This observation is consistent with enrichment of the same processes in downregulated HL temporal clusters in Col-0 (see above; Data S2) and supports our suggestion that in wild-type plants, downregulation of basal immunity may be a necessary prerequisite for successful adjustment to elevated light intensities and that *BBX32* is a negative regulator of this process.

BBX32 overexpression under LL and HL conditions perturbed the expression of PhAGs (Figure 6a; Data S8) and

the combined effects of such disruption would be consistent with a modestly significant ($P < 0.1$) depressed PSII quantum efficiency that both *BBX32*-OE lines displayed after a single 4 h of HL (Data S7).

BBX32 and the control of photosynthetic capacity and HL acclimation

There was an inhibitory effect of *BBX32* overexpression in HL on *GPT2* transcript levels (Figure 6c) and on those of *LHCB4.3* in *BBX32*-OE HL and LL plants (Figure 6a; Data S8). *GPT2* is required for dynamic acclimation (Athanasiou et al., 2010) and levels of LHCB4.3 correlate with the degree of long-term acclimation to HL (Albanese et al., 2016). This indicates that processes that would lead to acclimation had been initiated during this first exposure to HL and that *BBX32* is involved in their regulation. However, a single exposure to 4 h HL is not sufficient to induce HL acclimation and increased photosynthetic capacity. This requires, under our conditions, a further three daily episodes of 4 h HL for this to begin to occur (Figure 2a–d). Our experience is consistent with a previous study where dynamic acclimation took about 5 days to be fully manifested and 2–3 days to discern any change in photosynthesis rates after a permanent shift from a PPFD of 100–400 μmol m^{-2} sec^{-1} (Athanasiou et al., 2010). In contrast to the weak but significant effects on photosynthesis of *BBX32* overexpression during a single 4 h HL exposure (Data S7), there was a strongly significant negative impact upon HL acclimation after 5 days of daily 4 h HL (Figure 4a,c). This suggests that *BBX32* exerted a negative control on HL acclimation that was stronger than its impact on photosynthesis at growth PPFD. Similarly, a *gpt2* mutant showed wild-type levels of maximal photosynthetic capacity when grown at two different PPFDs (100 and 400 μmol m^{-2} sec^{-1}) but lowered dynamic acclimation going from the lower to the higher PPFD (Athanasiou et al., 2010). In summary, we propose that *BBX32* exerts control over a large number of genes in the first hours of HL exposure and the acclimation-associated increase in photosynthetic capacity that occurs several days later. Therefore, *BBX32* provides a link between these temporally distinct events that establish acclimation to HL (Eberhard et al., 2008; see Introduction).

Negative regulation of HL acclimation by *BBX32* (Figure 4a) suggested that a defective allele ought to confer a converse elevated phenotype. The mutant *bbx32-1* (see Results; Holtan et al., 2011), displayed a weakly significant trend of enhanced PSII operating efficiency compared with Col-0 between days 2 and 4 of the 5 days of 4-h HL exposure (Figure 4b; Data S7). However, this genotype is unlikely to be a null mutant. The mutagenic T-DNA is inserted such that the first 172 amino acid residues of BBX32 would still be produced and a truncated transcript spanning this region has been detected in *bbx32-1* seedlings (Holtan et al., 2011). The retained N-terminal region coded by this allele harbours the single B-Box zinc finger domain of BBX32 (Gangappa and Botto, 2014) and downstream sequences to residue 88, capable of binding at least the transcription regulator EMBRYONIC FLOWER1 (EMF1; Park et al., 2011). The possibility of a partially functional truncated BBX32 may explain the weak phenotype of *bbx32-1* with respect to this acclimation phenotype (Figure 4b; Data S7) and its mild constitutive photomorphogenic phenotype in seedlings (Holtan et al., 2011).

Establishment of HL acclimation involves BBX32-centric GRN members

The VBSSM that led us to *BBX32* also led us to *HY5* (Figure 3) and was subsequently reinforced by its known interaction with *BBX32* in seedling photomorphogenesis (Gangappa and Botto, 2016; Holtan et al., 2011). *HY5* was shown to be a strong positive regulator of acclimation in mature leaves (Figure 8d,e). Therefore, these observations reveal new functions for *BBX32* and *HY5*, extending their role to a further dimension in the interaction of the plant with its light environment. In seedlings, *HY5* controls chlorophyll content and transcript levels of PhAGs in cool temperatures (Toledo-Ortiz et al., 2014) and the control of chloroplast development during photomorphogenesis (Ruckle et al., 2007), which suggests, along with data shown here (Figure 6; Data S8), that control of these photosynthesis-associated processes by a *BBX32/HY5*-regulatory module is retained throughout the life of the plant.

SPA1, *PIF4*, and *PIF7* also were incorporated into the *BBX32*-centric GRN by VBSSM (Figure 3). This reinforced the comparison between the control of seedling photomorphogenesis and HL acclimation in fully expanded leaves, which was extended beyond the GRN by establishing that *CRY1* (and possibly *PHYB*) along with and one or more members of the *PIF* family are positive regulators of HL acclimation (Figures 8a,c and 9e), while *COP1* and one or more *SPA* genes are negative regulators (Figure 9b,c).

We suggest that *COP1* and *SPA* genes act together to suppress HL acclimation under LL by enabling the ubiquitin-mediated degradation of HY5 and therefore coupling photosynthetic capacity to the prevailing PPFD. In HL, this suppression would be reversed by CRY1 physically interacting with and inhibiting the action of COP1/SPA (Gangappa and Botto, 2016; Hoecker, 2017; Huang et al., 2014; Lau and Deng, 2012; Lau et al., 2019; Laubinger et al., 2004; Lian et al., 2011; Pham et al., 2018). Consequently, CRY1 would cause HY5 to be redirected to HL acclimation. However, a further adaptation may be required to retard or accelerate acclimation. For example, to fine tune the establishment of HL acclimation in a fluctuating light environment in order to balance source-sink relationships. We suggest under HL, when *HY5* is free of negative regulation by *COP1/SPA*, that *BBX32* is the important additional

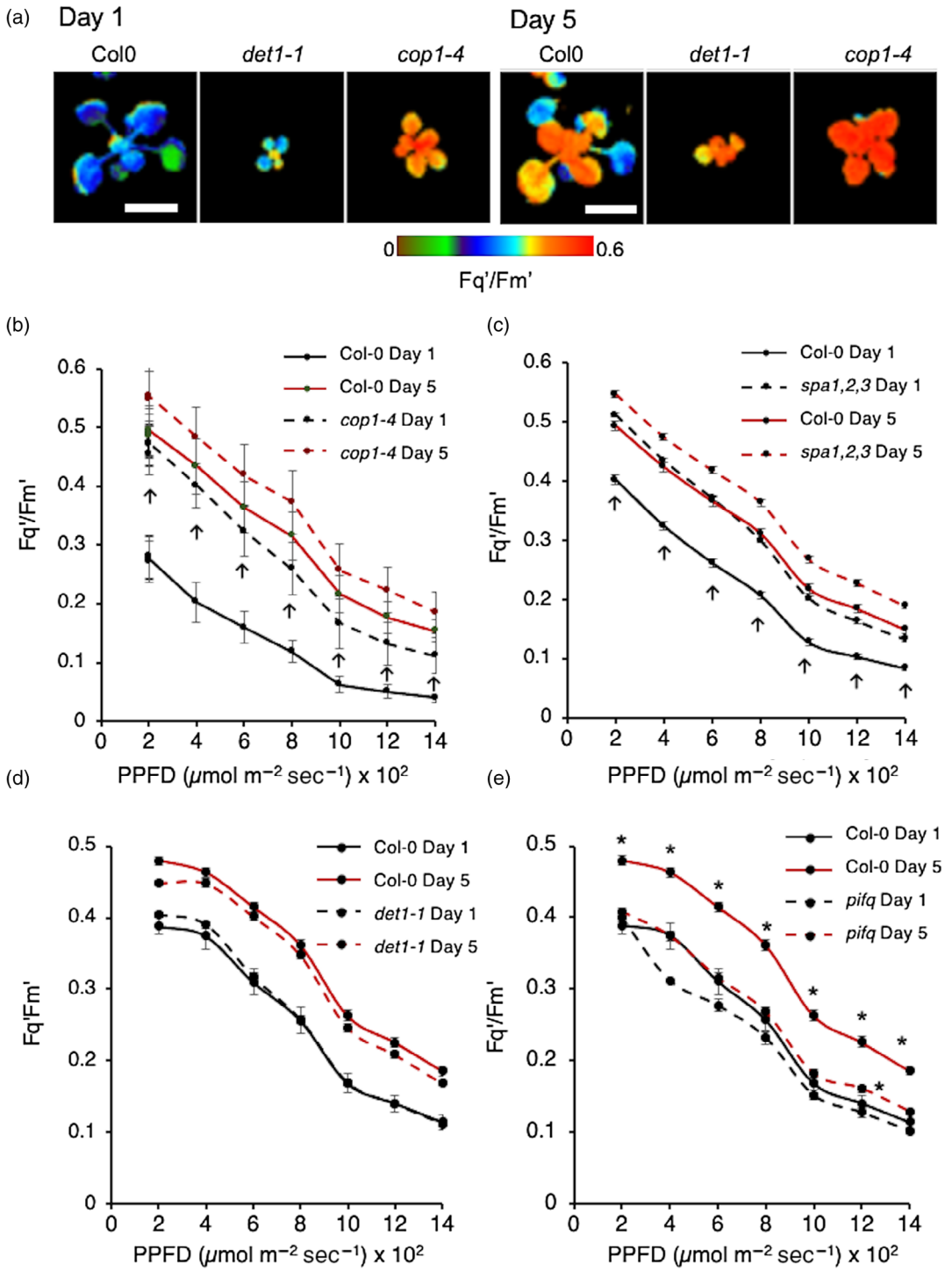

Figure 9. High light (HL) acclimation of photoreceptor signal transduction mutants.
(a) Photosynthetic efficiency of the same single Col-0, *cop1-4*, and *det1-1* plants after 1 and 5 days of daily 4 h HL exposure. Chlorophyll fluorescence (CF) images are of Fq′/Fm′ (photosystem II operating efficiency) at a 400 μmol m^{-2} sec^{-1} actinic photosynthetically active photon flux densities (PPFDs).
(b–e) Plots show the photosystem II operating efficiencies (Fq′/Fm′) determined from CF images from eight plants (24–28 days post-germination) over two experiments (means ± SE). Plants had been exposed to 5 days of daily 4 h HL (see Experimental procedures and legend of Figure 2). Note that because of the size of the *cop1-4, pifq*, and *det1-1* plants, data were collected from whole rosettes rather than from mature leaves. CF parameter values were collected at a range of actinic PPFDs at the end of days 1 and 5 of HL. Fq′/Fm′ values at day 1 (black lines) and day 5 (red lines) for mutant plants (dashed line) and Col-0 (solid line) of the HL treatments for (b) *cop1-4*, (c) *spa1,2,3*, (d) *det1-1*, and (e) *pifq*. Asterisks (e) indicate significant difference between mutant compared with Col-0 at day 5 ($P < 0.01$; ANOVA and Tukey HSD). Upward arrows (b,c) indicate significant difference between mutants and Col-0 at day 1 ($P < 0.01$; ANOVA and Tukey HSD).

moderator of the establishment of acclimation. The transcriptional control of *HY5* and by extension, other members of the *BBX32*-centric GRN (Figure 3), could be subject to regulation by additional intracellular signals in HL, such as those from chloroplasts (e.g. H_2O_2) and hormones, to coordinate a wider range of cellular processes necessary for acclimation (Dietz, 2015; Estavillo et al., 2011; Exposito-Rodriguez et al., 2017; Galvez-Valdivieso et al., 2009; Gangappa and Botto, 2016; Guo et al., 2016; Hardtke et al., 2000; Ramel et al., 2012, 2013). Other than *SPAs*, *HY5*, and *PIFs*, we have not determined if other GRN members (Figure 3) influence aspects of photosynthesis but *GOLDEN-LIKE 2* (*GLK2;* Waters et al., 2009) and *ACTIVATING FACTOR1* (*ATAF1*; also called *NO APICAL MERISTEM/CUP SHAPED COTYLEDON2* (NAC002); Garapati et al., 2015) do affect PhAG expression and chlorophyll levels.

The opposing regulation of HL acclimation by *BBX32* and *HY5* could mean that some form of interaction between these genes drives its establishment in a manner similar to their respective negative and positive regulation of photomorphogenesis (Datta et al., 2007; Gangappa and Botto, 2016; Holtan et al., 2011; Xu et al., 2014). BBX32 does not bind DNA and has been proposed to act as (co-) TF in complexes with several TFs, such as the BBX32-BBX21-HY5 tripartite complex involved in the control of photomorphogenesis (Datta et al., 2007; Gangappa and Botto, 2016; Holtan et al., 2011; Park et al., 2011; Tripathi et al., 2017; Xu et al., 2014). Therefore, there may also be a post-translational control of HY5 by BBX32 during HL acclimation.

The proposed need for both a *CRY1/COP1/SPA*- and a *BBX32*-mediated control of photosynthetic capacity and acclimation comes also from considerations about light quality and intensity. First, the fluence of blue light in the HL exposure used in this study would exceed the saturation of CRY1 activation, which is approximately 32–40 μmol m^{-2} sec^{-1} blue light (Hoang et al., 2008; Liu et al., 2020). Therefore, while CRY1 signalling would need to be activated (i.e., on) for acclimation to happen, further signalling input may be required from other sources via *BBX32* and its GRN to modulate the degree of response. A second factor is that at high fluence, CRY1 may produce H_2O_2 in the nucleus (Consentino et al., 2015). H_2O_2 for HL signalling is primarily synthesized and exported from chloroplasts and is dependent upon active photosynthetic electron transport (Exposito-Rodriguez et al., 2017; Mullineaux et al., 2018). However, this does not exclude the possibility that HL-dependent accumulation of H_2O_2 in nuclei for signalling may be augmented from other sources such as photo-saturated CRY1.

In contrast to Arabidopsis grown at differing PPFDs but using similar fluorescent lighting to this study (Walters et al., 1999; see Experimental procedures), no influence of *PHYA* or *PHYB* was observed on HL acclimation (Figure S6a,b). This could have been a consequence of the degree of blue light used in both growth conditions and in HL exposure (9% and 58% of the total PPFD respectively; Figure S7; see Experimental procedures). This range of wavelengths in artificial lighting is typical of many controlled environment conditions (Naznin et al., 2019) and may have favoured a response mediated by *CRY1*. The observation that plants harbouring a constitutively active *PHYB* allele (*YHB*) displayed a partially accelerated acclimation phenotype (Figure 8c) means that PHYs could also control HL acclimation under some light environments and modify or interact with a *CRY1*-dependent signalling pathway (Ahmad et al., 2002; Yu et al., 2010).

Conundrum of the control of photosynthetic capacity and the type of HL acclimation

In interpreting the data from the mutants and *BBX32*-OE genotypes used in this study, the question can be asked: Is the mutants' altered HL acclimation phenotype a consequence of limited development or functioning of the photosynthetic apparatus such that maximal photosynthetic capacity could never be attained? This question can be answered in two parts: first and as stated above, the effect of *BBX32* overexpression is more marked in the increase in photosynthetic efficiency between days 1 and 5 of daily HL exposures (i.e. HL acclimation) than in the starting photosynthetic efficiencies at day 1 (Figure 4a,c; Data S7). The same pattern can be observed in the *hy5* mutants (Figure 8d,e; Data S7). However, the *cry1* mutants and *pifq* showed no difference from Col-0 on day 1 HL but a strong difference by day 5 HL (Figures 8a,b and 9e). Second, mutants such as *bbx32-1*, *YHB*, *cop1-4*, and *spa1,2,3* displayed an accelerated chloroplast-level HL acclimation phenotype, which showed that their photosynthetic apparatus was set at a level higher than it should have been for their growth PPFD and for the number of days of 4-h HL exposure (Figures 4b, 8c and 9a–c). This means that HL acclimation can become uncoupled from the prevailing light intensity. However, in such mutants this phenotype cannot be due to partially disabled photosynthesis but is a feature of acclimated wild-type plants having been exposed to HL for a longer period. Therefore, in summary, we conclude that *BBX32*, members of its GRN and *CRY1* exert both negative and positive control over the setting of photosynthetic capacity *and* the extent of chloroplast-level acclimation to HL.

HL acclimation in fully expanded leaves strongly suggests *BBX32* regulates dynamic acclimation (see Introduction) possibly, but not exclusively, through the control of *GPT2* expression (Figure 6c; Athanasiou et al., 2010). However, we cannot rule out that *BBX32*, its GRN and *CRY1*-directed signalling influence developmental acclimation (see Introduction) as many of the mutants used in this study have altered growth and development phenotypes

(Gangappa and Kumar, 2018; Holtan et al., 2011; Jones et al., 2015; Laubinger et al., 2004; Leivar et al., 2008; Ruckle et al., 2007; Figure 9a). However, such an effect would probably not influence chloroplast-level acclimation as this property was unaffected in *det1-1* plants despite their severe dwarf shoot morphology (Figure 9a,d).

In summary, this study uncovering a *BBX32*-centric GRN provides the outline for a highly sensitive and flexible system of adjusting photosynthetic capacity and points to how chloroplast-level acclimation is influenced not only by light intensity and quality but also many other environmental and internal cues.

EXPERIMENTAL PROCEDURES

Growth conditions

Plants were grown in an 8-h photoperiod (short day) at a PPFD of 150 ($\pm$10) μmol m^{-2} sec^{-1} under fluorescent tubes (Philips TLD 58W, 830 (warm whites); the spectrum of the light source is shown in Figure S7), 22 $\pm$ 1°C, 1-kPa vapour pressure deficit and cultivation conditions as described previously (Bechtold et al., 2016; Windram et al., 2012). Unless stated otherwise, all plants were used from 35 to 40 dpg.

Arabidopsis genotypes

The following Arabidopsis mutants and transgenic lines, all in a Col-0 background, have been described previously: BBX32-10, BBX32-12, *bbx32*-1 (Holtan et al., 2011), *hy5*-215 (Oyama et al., 1997), *hy5*-2 (Ruckle et al., 2007), *pifq* (Leivar et al., 2008), *cop1-4* (Deng and Quail, 1992), *det1-1* (Chory et al., 1989), *spa1/spa2/spa3* (*spa*1,2,3; Laubinger et al., 2004), *phyA-219* (Reed et al., 1994), *phyB*-9 (Yoshida et al., 2018), *cry1-304* (Ahmad and Cashmore, 1993), *cry2-1* (Guo et al., 1998), and *phyBY276H* (*YHB*; Jones et al., 2015).

Identification of the cry1M32 mutant

Based upon earlier research in our laboratory (Galvez-Valdivieso et al., 2009; Gorecka et al., 2014) in which we studied a possible role for heterotrimeric G protein-mediated HL signalling, we set out to identify candidate genes coding for seven transmembrane proteins that may have a role as G protein-coupled receptors. A collection of 59 T-DNA insertion mutants in genes coding for putative 7-transmembrane proteins (Moriyama et al., 2006; a kind gift from Professor Alan Jones, University of North Carolina) was screened for perturbed CF in response to HL exposure (see below). The screening revealed that the insertion line Sail_1238_E12 (hereafter termed M32) was deficient in HL acclimation (Figure 8b). The information available on T-DNA flanking sequences indicated that this was a T-DNA insertion in the first exon of At4g21570, a gene encoding a transmembrane protein of unknown function. However, complementation of M32 by transformation with the wild-type At4g21570 gene did not restore a wild-type phenotype.

Besides being defective in dynamic acclimation, M32 was impaired in blue light inhibition of hypocotyl elongation under both low and high blue light fluence, accumulated less chlorophylls and anthocyanins than Col-0 under blue light, and presented delayed flowering time when grown in short day photoperiod. (Figure S8b–e). Later and in light of our subsequent hypothesis that *CRY1*-mediated signalling controls HL acclimation in Arabidopsis (see Results and Discussion), we realized that M32 resembled the phenotype of known *cry1* mutants. Therefore, we tested if *CRY1* was altered in this mutant. *CRY1* was amplified from its genomic DNA and the PCR product was Sanger sequenced on both strands. Col-0 *CRY1* amplicon was also sequenced. The analysis of the sequence showed that in M32, *CRY1* contains a single point mutation (G→A), which caused a substitution of $Gly_{347}Arg$ mutation in CRY1 (Figure S8f). This mutation was previously identified in a screening of EMS-mutagenized Arabidopsis seedlings (Ahmad et al., 1995) and designated as *hy4-15*, and affects the domain comprising the photolyase signature sequence. Consequently, *hy4-15* plants produce a wild-type amount of full-length CRY1, but the protein is not functional. Therefore, we concluded that the M32 mutant is in fact a *cry1* mutant that we named *cry1M32*.

HL exposures

The HL exposure was a PPFD of 1100 ($\pm$100) μmol m^{-2} sec^{-1} from a white light emitting diode (LED) array (Isolight 4000; Technologica Ltd, Colchester, UK) as described previously (Gorecka et al., 2014) and permitted the simultaneous exposure of nine plants. The spectrum of the LED array is shown in Figure S7.

For the HL time-series transcriptomics, two consecutive sowings, 24 h apart, were grown to 35 dpg on the same growth room shelf and randomized across the shelf every day. Leaf 7 (Bechtold et al., 2016) was tagged at 30 dpg. We used this staging of plant growth and 3 LED Isolight arrays to treat 27 plants each day. The HL exposure began 1 h after subjective dawn and was completed 1 h before subjective dusk. Each set of tagged leaves (four) at each HL time point and their LL controls (four) were sampled within 5 min at time 0.5 h and each 0.5 h interval for the 6 h exposure. Two HL experiments were conducted with duplicate samplings of a full range of time points on each day. In addition, four time zero samples were processed for the 0 h time point. Both HL experiments provided, in total, 100 samples for RNA extraction. These were four biological replicates (i.e. four sampled leaves) per time point per HL treatment (48 samples) and LL control (48 samples) plus four 0 time point samples.

To elicit HL acclimation, plants were subjected to 4 h HL, followed by a 0.5 h dark adaptation and then exposed to a range of actinic PPFDs (over 50 min) to collect CF data (see below). This HL treatment was repeated daily and CF data collected from the same plants for 5 consecutive days or on days 1 and 5 only as stated.

CF measurements and imaging

During the time-series HL experiments, CF measurements were taken from leaf 7 of one plant *in situ* under each isolight using PAM-2000 portable modulated fluorimeters (PAM-2000; Walz GmbH, Effeltrich, Germany). At the end of each experiment the dark-adapted CF parameter Fv/Fm was determined for the same plants and LL controls and then again 24 h after being returned to growth conditions.

For the HL acclimation experiments, photosynthetic efficiency was estimated with a CF imaging system (Fluorimager; Technologica Ltd), exposing the plants to increasing actinic PPFD from 200 to 1400 μmol m^{-2} sec^{-1} in 200 μmol m^{-2} sec^{-1} steps every 5 min as described previously (Barbagallo et al., 2003; Gorecka et al., 2014). Whole rosette CF images were collected at each PPFD and processed using software (Technologica Ltd) to collect numerical data typically from fully expanded leaves ($\geq$ 4 per plant) for Fq′/Fm′, Fv′/Fm′ and Fq′/Fv′ (Baker, 2008; Barbagallo et al., 2003; Gorecka et al., 2014). In some experiments, the diminished size of mutant plants rendered image processing problematic and

in such stated cases, whole rosette data were collected. The raw data were fed via Excel into a program in R to calculate, plot, and analyse statistically the CF parameters (Gorecka et al., 2014). The fluorimager software produces average data of all leaf pixel values. CF parameters were represented as mean ± SE from a minimum of four plants, and statistical significance was estimated with ANOVA followed by a *post-hoc* Tukey HSD test.

Measurement of photosynthesis

A was measured on leaf 7 of plants at 49 dpg using an infrared gas exchange system (CIRAS-1; PP Systems, Amesbury, MA, USA). The response of *A* to changes in the intercellular CO_2 concentration (C_i) was measured under a saturating PPFD, provided by a combination of red and white LEDs (PP Systems, Amesbury, MA, USA). In addition, the response of *A* to changes in PPFD from saturating to subsaturating levels was measured using the same light source at the current atmospheric CO_2 concentration (390 μmol mol^{-1}). All gas analysis was made at a leaf temperature of 20 ± 1°C and a VPD of 1 ± 0.2 kPa. Plants were sampled between 1 and 4 h after the beginning of the photoperiod. For each leaf, steady-state rates of *A* at current atmospheric [CO_2] were recorded at the beginning of each measurement.

Relative ion leakage

The method described by Overmyer et al. (2008) was followed. Briefly, leaves were collected from plants and placed in 5 ml deionized water, incubated with rotary shaking (100 rpm) for 4 h, and the conductivity of the solution determined with a conductivity meter (Mettler Toledo, Leicester, UK) calibrated according to the manufacturer's instructions. Leaves were frozen overnight, thawed, and conductivity measured again. Relative ion leakage was expressed as conductivity after 4 h/conductivity after freeze-thawing.

RNA extraction, labelling and hybridization to microarrays

For the time-series HL experiment, RNA was extracted from leaf 7 samples, labelled and hybridized to CATMA (a Complete Arabidopsis Transcriptome MicroArray) microarrays (v3; Sclep et al., 2007), as described by Breeze et al. (2011). Two technical replicates were used per biological replicate. Four biological replicates with, in total, 13 time points per treatment (HL and LL) were analysed in this way, resulting in a highly replicated high-resolution time series of expression profiles. The experimental procedure for the hybridization of labelled cDNA samples for the HL and LL time series followed a statistically randomized loop design (Figure S9), which enabled expression to be determined at different time points both within and between treatments. After hybridization and washing, microarrays were scanned for Cy3 and Cy5 fluorescence and analysed as below. The raw and processed data are deposited with NCBI GEO (GSE78251).

Analysis of microarray data

This has been described in detail previously (Breeze et al., 2011; Windram et al., 2012). Briefly, a mixed model analysis using MAANOVA (Breeze et al., 2011; Wu et al., 2003) was used with the same random (dye and array slides) and fixed variables (time point, treatments, and biological replicate) to test the interaction between these factors for the analysis of time-series microarray data for senescing, *Botrytis cinerea*-infected, *Pseudomonas syringae*-infected and drought-stressed leaves (Bechtold et al., 2016; Breeze et al., 2011; Lewis et al., 2015; Windram et al., 2012). Predicted means were calculated for each gene probe for each of the combinations of treatment, biological replicate, and time point, and for each of the combinations of treatment and time point from averages of the biological replicates.

A GP2S Bayes' factor (Stegle et al., 2010) was used to rank probes and genes in order of likelihood of differential expression over the whole of the time series. Inspection of selected probes from the rank order of likelihood of differential expression was used to identify significant changes in expression with a Bayes' factor cut-off >10 giving 4069 probes corresponding to 3844 DEGs (Data S1).

Clustering of gene expression profiles

The expression patterns of the identified DEGs in HL and LL were co-clustered with SPLINECLUSTER (Heard et al., 2005), using the mean expression profiles of the biological replicates generated from MAANOVA and a previous precision value of 0.001, as described previously (Bechtold et al., 2016; Windram et al., 2012).

GO analysis

GO annotation analysis was performed using DAVID (Huang et al., 2008) or AGRIGO (Du et al., 2010) with the GO Biological Process (BP) category (Ashburner et al., 2000). Overrepresented GO_BP categories were identified using a hypergeometric test with an FDR threshold of 0.05 compared against the whole annotated genome as the reference set.

Comparisons with published transcriptomics data

The 3844 HL DEGs were compared on a cluster-by-cluster basis with publicly available transcriptomics data. The references for each dataset can be found in the References. Each DEG list from published data was mapped to AGI codes when necessary, cleaned to obtain single AGI codes since in some microarray data, probes mapped to several genes or were listed as 'no_match' and were eliminated from the list. Overlaps within each cluster and their statistical significance were determined using a Hypergeometric Distribution Test [phyper function in R (v3.2.1)] in a custom R script, available upon request. When required, Venn diagrams of overlaps between datasets were plotted with Venny (http://bioinfogp.cnb.csic.es/tools/venny/index.html) and the significance of the overlaps calculated using the R phyper function.

VBSSM

A full description of VBSSM applied to this type of time-series transcriptomics data is provided in Bechtold et al. (2016). The individual expression data for each biological replicate ($n = 4$) for selected DEGs in HL was run through the VBSSM algorithm (Beal et al., 2005) on a local server at the University of Essex (Bechtold et al., 2016) to generate the GRNs as described in Results. The VBSSM output files were imported, mapped, and plotted with CYTOSCAPE (Shannon et al., 2003; http://www.cytoscape.org/).

Expression profiling by RNA-seq

Total RNA was extracted from mature leaves of each individual shoot giving four biological replicate samples per treatment and genotype. The RNA was quality controlled as previously described (Albihlal et al., 2018). Library construction after mRNA enrichment and double-stranded cDNA synthesis carried out using Illumina protocols by Novogene (UK) Ltd (Cambridge, UK; en.novogene.com/). Library sequencing was carried out on an Illumina HiSeq 4000 with a 150-bp end reads to a depth of 20 million. Extraction

and quality control of data from raw fastq files were carried out using the program CASAVA (Hosseini et al., 2010). The mapping of reads to the TAIR10 Arabidopsis genome sequence, followed by sorting and indexing of BAM output files was carried out using default settings in the program HISAT2 (v2.0.5; Kim et al., 2015). Across all samples, >92.5% of bases read attained the Q30 score threshold. Transcript assembly and quantification was as fragments per kilobase of transcript sequence per million base pairs sequenced using HTseq (in union mode; Anders et al., 2015). Determination of differential expression between different genotypes and treatments was done using the program DESEQ2 (Love et al., 2014) after read count normalization and an adjusted *P* value threshold of <0.05 (negative binomial distribution *P* value model and Benjamini–Hochberg correction for multiple testing). Raw and processed data files were deposited in NCBI Gene Expression Omnibus (GSE158898).

Locus codes of genes mentioned in the paper

AT1G01720, *ATAF1*; AT1G04400, *CRY2*; AT1G06180, *MYB13*; AT1G09100, *AAA-ATPase*; AT1G09570, *PHYA*; AT1G14150, *PnsL2*; AT1G14920, *GAI*; AT1G16300, *GAPCP-2*; AT1G22190, *RAP2.4*; AT1G22640, *MYB3*; AT1G25540, *PFT1*; AT1G25550, *MYB-like*; AT1G29910, *Lhcb1*/CAB3; AT1G29920, *CAB2/LHCII*; AT1G29930, *CAB1/LHCII*; AT1G43670, *FBPASE*; AT1G44575, *PsbS*; AT1G49720, *ABF1*; AT1G50420, *SCL3*; AT1G50640, *ERF3*; AT1G61800, *GPT2*; AT1G68520, *BBX14*; AT1G69010, *BIM2*; AT1G69490, *NAP*; AT1G70000, *MYBD*; AT1G75540, *BBX21*; AT1G76100, *PETE1*; AT1G76570, *LHCB7*; AT1G77450, *NAC032*; AT1G79550, *PGK*; AT2G01290, *RPI2*; AT2G05070, *LHCB2*; AT2G18790, *PHYB*; AT2G21330, *FBA1*; AT2G24540, *AFR*; AT2G24790, *BBX4*; AT2G27510, *FD3*; AT2G28350, *ARF10*; AT2G30790, *PSBP-2*; AT2G32950, *COP1*; AT2G34430, *LHB1B1*; AT2G34720, *NF-YA4*; AT2G35940, *BLH1*; AT2G40100, *LHCB4.3*; AT2G40970, *MYBC1*; AT2G43010, *PIF4*; AT2G46270, *GBF3*; AT2G46340, *SPA1*; AT3G08940, *LHCB4.2*; AT3G09640, *APX2*; AT3G21150, *BBX32*; AT3G27690, *LHCB2.3*; AT3G60750, *TK*; AT3G61190, *BAP1*; AT4G05180, *PSBQ-2*; AT4G05390, *RFNR1*; AT4G08920, *CRY1*; AT4G10180, *DET1*; AT4G10340, *LHCB5*; AT4G15090, *FAR1*; AT4G17460, *HAT1*; AT4G29190, *OZF2*; AT4G32730, *PC-MYB1*; AT4G38960, *BBX19*; AT5G01600, *FER1*; AT5G07580, *ERF106*; AT5G08520, *MYBS2*; AT5G11260, *HY5*; AT5G11530, *EMF1*; AT5G12840, *NF-YA1*; AT5G15210, *HB30*; AT5G28450, *LHC1*; AT5G38420, *RBCS2B*; AT5G38430, *RBCS1B;* AT5G42520, *BPC6*; AT5G43270, *SPL2*; AT5G44190, *GLK2*; AT5G51190, *ERF105*; AT5G61270, *PIF7*; AT5G61590, *ERF107*; AT5G62000, *ARF2*; AT5G65310, *HB5*; AT5G67300, *MYBR1*; AT5G67420, *LBD37*; ATCG00020, *PSBA*; ATCG00270, *PSBD*; ATCG00300, *PSBZ*; ATCG00350, *PSAA*.

ACKNOWLEDGEMENTS

We thank Silvere Vialet-Chabrand and Steven Driever for discussions and advice on statistical and physiological aspects of the study. We thank Laura Flanders and Rahjish Khanna for the *BBX32*-OE lines and *bbx32-1*. We acknowledge European (Nottingham) Arabidopsis Stock Centre for providing *cry1-304*, *cry2-1*, *phyA-219*, *phyB-9*, *pifq*, *pif4-1*, *lhy-21*, and *det1-1*. Matthew Jones and Ute Hoecker respectively are gratefully acknowledged for providing seed of *cop1-4*, Col-0 *YHB*, and *spa1/spa2/spa3*. This work was supported by the UK Biotechnology and Biological Sciences Research Council (grants BB/F005822/1 and BB/F005806/1). CAP and DLW were supported by the UK Engineering and Physical Science Research Council (grant EP/I036575/1). JSAM was supported by NERC-CASE award (ENV-EATR-DTP: NE/L002582/1).

AUTHOR CONTRIBUTIONS

PMM, UB, GGV, and RAF carried out the HL time-series experiments and RNA extractions. PMM, RAF, and EJS conducted the CF measurements for HL responses and dynamic acclimation. MER carried out the RNA extractions and with EJS and PMM, conducted the RNA-seq data analysis. TL designed the gas exchange measurements, which were performed by JSAM and PAD. CAP, LB, JDM, AM, RAF, and PMM were responsible for microarray data generation and analysis. RAF and PMM conducted the VBSSM modelling under the guidance of CAP. PMM, KJD, DLW, JB, VB-W, and UB developed the HL time-series project. PMM conceived and wrote the manuscript with contributions from all authors.

CONFLICT OF INTEREST

EJS and PMM declare a GB patent application for part of the work reported here. The remaining authors declare that they have no competing interests.

DATA AVAILABILITY STATEMENT

Complete microarray datasets are deposited at GEO under GSE78251, GSE87755 and GSE87756. RNA-seq datasets are also deposited at GEO under GSE158898.

SUPPORTING INFORMATION

Additional Supporting Information may be found in the online version of this article.

Figure S1. Examples of temporal differentially expressed clusters.

Figure S2. Comparison of plants exposed to daily HL for 5 days with their equivalent age LL controls and induction of HL acclimation in older plants.

Figure S3. HL exposure used does not produce extensive photodamage to leaves.

Figure S4. First draft inferred HL gene regulatory network and HL acclimation in *lhy-21* plants.

Figure S5. Temporal patterns of transcript abundance of the 12 most connected genes in the BBX32-centric GRN under LL and HL conditions

Figure S6. HL acclimation of *phyB-9*, *phyA-211*, *cry2-1*, and *pif4-2* plants compared with Col-0.

Figure S7. Spectral properties of the growth lights and isolight used for HL exposure.

Figure S8. Identification and characterization of *cry1*-M32.

Figure S9. Randomized loop design employed for loading samples on to the two-channel CATMA arrays.

Data S1. The 3844 HL DEGs on a cluster-by-cluster basis.

Data S2. Significantly enriched Biological Process GO Terms for the HL DEGs in each temporal cluster.

Data S3. Differentially expressed genes from leaf 7 of Arabidopsis subjected to a 30-min temperature rise from 22 to 27°C under LL and HL conditions.

Data S4. Significant overlaps, on a cluster-by-cluster basis, between publicly available gene expression datasets and transcriptomic meta-analyses for mutants and treatments that perturb

chloroplast-nucleus signalling, ROS metabolism or are undergoing dynamic acclimation.

Data S5. Statistical data for CF measurements of 24–28 dpg Col-0 plants and 44–48 dpg Col-0 plants undergoing HL acclimation.

Data S6. Annotated transcription (co-)factor genes differentially expressed in HL versus LL leaves.

Data S7. Photosynthetic efficiency of *BBX32*-OE, *bbx32-1*, *hy5-2*, and *hy5-215* plants during induction of dynamic acclimation.

Data S8. FKPM values for transcripts coding for (a) (co-)TFs in the inferred gene regulatory network in Figure 3 and (b) photosynthesis-associated nuclear- and plastid-encoded genes.

Data S9. Transcripts that show a significant change in response to 3.5 h HL in Col-0 and/or in *BBX32*-OE LL and HL plants.

Data S10. Significantly enriched GO BP Terms common between *BBX32*-OE LL/Col-0 LL, *BBX32*-OE HL/Col-0 HL and HL/LL Col-0 DEGs.

Data S11. DEGs in the GO BP terms common between BBX32-OE/Col-0 LL, *BBX32*-OE HL/Col-0 HL and from the HL time-series clusters.

REFERENCES

Adamiec, M., Drath, M. & Jackowski, G. (2008) Redox state of plastoquinone pool regulates expression of *Arabidopsis thaliana* genes in response to elevated irradiance. *Acta Biochimica Polonica*, **55**, 161–173.

Adams, W.W. III, Cohu, C.M., Amiard, V. & Demming-Adams, B. (2014) Associations between the acclimation of phloem-cell wall ingrowths in minor veins and maximal photosynthesis rate. *Frontiers in Plant Science*, **5**, 24.

Ahmad, M. & Cashmore, A.R. (1993) HY4 gene of *A. thaliana* encodes a protein with characteristics of a blue-light photoreceptor. *Nature*, **366**, 162–166.

Ahmad, M., Grancher, N., Heil, M., Black, R.M., Giovani, B., Galland, P. *et al.* (2002) Action spectrum for cryptochrome-dependent hypocotyl growth inhibition in Arabidopsis. *Plant Physiology*, **129**, 774–785.

Ahmad, M., Lin, C. & Cashmore, A.R. (1995) Mutations throughout an *Arabidopsis* blue-light photoreceptor impair blue-light-responsive anthocyanin accumulation and inhibition of hypocotyl elongation. *The Plant Journal*, **8**, 653–658.

Albanese, P., Manfedi, M., Meneghesso, A., Marengo, E., Saracco, G., Barber, J. *et al.* (2016) Dynamic reorganization of photosystem II supercomplexes in response to variations in light intensities. *Biochimica et Biophysica Acta*, **1857**, 1651–1660.

Albihlal, W.S., Obomighie, I., Blein, T., Persad, R., Chernukhin, I., Crespi, M. *et al.* (2018) Arabidopsis *HEAT SHOCK TRANSCRIPTION FACTORA1b* regulates multiple developmental genes under benign and stress conditions. *Journal of Experimental Botany*, **69**, 2847–2862.

Allahverdiyeva, Y., Battchikova, N., Brosché, M., Fujii, H., Kangasjärvi, S., Mulo, P. *et al.* (2015) Integration of photosynthesis, development and stress as an opportunity for plant biology. *New Phytologist*, **208**, 647–655.

Anders, S., Pyl, P.T. & Huber, W. (2015) HTSeq–a Python framework to work with high-throughput sequencing data. *Bioinformatics*, **31**, 166–169. https://doi.org/10.1093/bioinformatics/btu638.

Ashburner, M., Ball, C.A., Blake, J.A., Botstein, D., Butler, H., Cherry, J.M. *et al.* (2000) Gene Ontology: tool for the unification of biology. *Nature Genetics*, **25**, 25–29.

Athanasiou, K., Dyson, E.C., Webster, R.E. & Johnson, G.N. (2010) Dynamic acclimation of photosynthesis increases plant fitness in changing environments. *Plant Physiology*, **152**, 366–373.

Badger, M.R., von Caemmerer, S., Ruuska, S. & Nakano, H. (2000) Electron flow to oxygen in higher plants and algae: rates and control of direct photoreduction (Mehler reaction) and rubisco oxygenase. *Philosophical Transactions of the Royal Society of London. Series B, Biological Sciences*, **355**, 1433–1446.

Baker, N.R. (2008) Chlorophyll fluorescence: a probe of photosynthesis in vivo. *Annual Review of Plant Biology*, **59**, 89–113.

Balfagón, D., Sengupta, S., Gómez-Cadenas, A., Fritschi, F.B., Azad, R.K., Mittler, R. & Zandalinas, S.I. (2019) Jasmonic acid is required for plant acclimation to a combination of high light and heat stress. *Plant Physiology*, **181**, 1668–1682.

Ball, L., Accotto, G.P., Bechtold, U., Creissen, G., Funck, D., Jimenez, A. *et al.* (2004) Evidence for a direct link between glutathione biosynthesis and stress defense gene expression in Arabidopsis. *The Plant Cell*, **16**, 2448–2462.

Barbagallo, R.P., Oxborough, K., Pallett, K.E. & Baker, N.R. (2003) Rapid, non-invasive screening for perturbations of metabolism and plant growth using chlorophyll fluorescence imaging. *Plant Physiology*, **132**, 485–493.

Beal, M.J., Falciani, F., Ghahramani, Z., Rangel, C. & Wild, D.L. (2005) A Bayesian approach to reconstructing genetic regulatory networks with hidden factors. *Bioinformatics*, **21**, 349–356.

Bechtold, U., Penfold, C.A., Jenkins, D.J., Legaie, R., Moore, J.D., Lawson, T. *et al.* (2016) Time-series transcriptomics reveals that *AGAMOUS-LIKE22* affects primary metabolism and developmental processes in drought-stressed Arabidopsis. *The Plant Cell*, **28**, 345–366. in press.

Berens, M.L., Wolinska, K.W., Spaepen, S., Ziegler, J., Nobori, T., Nair, A. *et al.* (2019) Balancing trade-offs between biotic and abiotic stress responses through leaf age-dependent variation in stress hormone cross-talk. *Proceedings of the National Academy of Sciences of United States of America*, **116**(6), 2364–2373.

Breeze, E., Harrison, E., McHattie, S., Hughes, L., Hickman, R., Hill, C. *et al.* (2011) High-resolution temporal profiling of transcripts during Arabidopsis leaf senescence reveals a distinct chronology of processes and regulation. *The Plant Cell*, **23**, 873–894.

Chen, D., Xu, G., Tang, W., Jing, Y., Ji, Q., Fei, Z. *et al.* (2013) Antagonistic basic helix-loop-helix/bZIP transcription factors for transcriptional modules that integrate light and reactive oxygen species signalling in *Arabidopsis*. *The Plant Cell*, **25**, 1657–1673.

Chory, J. & Peto, C.A. (1990) Mutations in the *DET1* gene affect cell-type-specific expression of light-regulated genes and chloroplast development in *Arabidopsis*. *Proceedings of the National Academy of Sciences of the United States of America*, **87**, 8776–8780.

Chory, J., Peto, C., Feinbaum, R., Pratt, L. & Ausubel, F. (1989) Arabidopsis thaliana mutant that develops as a light-grown plant in the absence of light. *Cell*, **58**, 991–999.

Consentino, L., Lambert, S., Martino, C., Jourdan, N., Bouchet, P.-E., Witczak, J. *et al.* (2015) Blue-light dependent reactive oxygen species formation by *Arabidopsis* cryptochrome may define a novel evolutionary conserved signaling mechanism. *New Phytologist*, **206**, 1450–1462.

Crisp, P.A., Ganguly, D.R., Smith, A.B., Murray, K.D., Estavillo, G.Z., Searle, I. *et al.* (2017) Rapid recovery gene downregulation during excess light stress and recovery in Arabidopsis. *The Plant Cell*, **29**, 1836–1863.

Datta, S., Hettiarachchi, C., Johansson, H. & Holm, M. (2007) SALT TOLERANCE HOMOLOG2, a B-Box protein in *Arabidopsis* that activates transcription and positively regulates light-mediated development. *The Plant Cell*, **19**, 3242–3255.

Deng, X.-W. & Quail, P.W. (1992) Genetic and phenotypic characterization of *cop*1 mutants of *Arabidopsis thaliana*. *The Plant Journal*, **2**, 83–95.

Díaz, M., De Haro, V., Muñoz, R. & Quiles, M.J. (2007) Chlororespiration is involved in the adaptation of *Brassica* plants to heat and high light intensity. *Plant, Cell and Environment*, **30**, 1578–1585.

Dong, J., Tang, D., Gao, Z., Yu, R., Li, K., He, H. *et al.* (2014) *Arabidopsis* DE-ETIOLATED1 represses photomorphogenesis by positively regulating phytochrome-interacting factors in the dark. *The Plant Cell*, **26**, 3630–3645.

Dietz, K.-J. (2015) Efficient high light acclimation involves rapid processes at multiple mechanistic levels. *Journal of Experimental Botany*, **66**, 2401–2414.

Driever, S. & Baker, N.R. (2010) The water-water cycle in leaves is not a major alternative electron transport sink for dissipation of excess excitation energy when CO_2 assimilation is restricted. *Plant, Cell and Environment*, **34**, 837–846.

Drozak, A. & Romanowska, E. (2006) Acclimation of mesophyll and bundle sheath chloroplasts of maize to different irradiances during growth. *Biochimica et Biophysica Acta*, **1757**, 1539–1546.

Du, Z., Zhou, X., Ling, Y., Zhang, Z. & Su, Z. (2010) agriGO: a GO analysis toolkit for the agricultural community. *Nucleic Acids Research*, **38**, W64–W70.

Eberhard, S., Finazzi, G. & Wollman, F.-A. (2008) The dynamics of photosynthesis. *Annual Review of Genetics*, **42**, 463–515.

Estavillo, G.M., Crisp, P.A., Pomsiriwong, W., Wirtz, M., Collinge, D., Carrie, C. *et al.* (2011) Evidence for a SAL1-PAP chloroplast retrograde pathway that functions in drought and high light signalling in *Arabidopsis*. *The Plant Cell*, **23**, 3992–4012.

Exposito-Rodriguez, M., Laissue, P.P., Yvon-Durocher, G., Smirnoff, N. & Mullineaux, P.M. (2017) Photosynthesis-dependent H_2O_2 transfer from chloroplasts to nuclei provides a high-light signalling mechanism. *Nature Communications*, **8**, 49.

Gadjev, I., Vanderauwera, S., Gechev, T.S., Laloi, C., Minkov, I.N., Shulaev, V. *et al.* (2006) Transcriptomic footprints disclose specificity of reactive oxygen species signaling in Arabidopsis. *Plant Physiology*, **141**, 436–455.

Galvez-Valdivieso, G., Fryer, M.J., Lawson, T., Slattery, K., Truman, W., Smirnoff, N. *et al.* (2009) The high light response in *Arabidopsis* involves ABA signaling between vascular and bundle sheath cells. *The Plant Cell*, **21**, 2143–2162.

Gangappa, S.N. & Botto, J.F. (2014) The BBX family of plant transcription factors. *Trends in Plant Science*, **19**, 460–470.

Gangappa, S.N. & Botto, J.F. (2016) The multifaceted roles of HY5 in plant growth and development. *Molecular Plant*, **9**, 1353–1365.

Gangappa, S.N. & Kumar, S.V. (2018) DET1 and COP1 modulate the coordination of growth and immunity in response to key seasonal signals in *Arabidopsis*. *Cell Reports*, **25**, 29–37.

Ganguly, D., Crisp, P., Harter, K., Pogson, B.J. & Albrecht-Borth, V. (2015) Genetic suppression of plant development and chloroplast biogenesis via the Snowy Cotyledon 3 and Phytochrome B pathways. *Functional Plant Biology: FPB*, **42**, 676–686.

Garapati, P., Xue, G.-P., Munné-Bosch, S. & Balazadeh, S. (2015) Transcription factor ATAF1 in Arabidopsis promotes senescence by direct regulation of key chloroplast maintenance and senescence transcriptional cascades. *Plant Physiology*, **168**, 1122–1139.

Gorecka, M., Alvarez-Fernandez, R., Slattery, K., McAusland, L., Davey, P.A., Karpinski, S. *et al.* (2014) Abscisic acid signalling determines susceptibility of bundle sheath cells to photoinhibition in high light-exposed *Arabidopsis* leaves. *Philosophical Transactions of the Royal Society of London. Series B, Biological Sciences*, **369**, 20130234.

Guo, H., Yang, H., Mockler, T.C. & Lin, C. (1998) Regulation of flowering time by Arabidopsis photoreceptors. *Science*, **279**(5355), 1360–1363.

Guo, Z., Wang, F., Xiang, X., Ahammed, G.J., Wang, M., Onac, E. *et al.* (2016) Systemic induction of photosynthesis via illumination of the shoot apex is mediated sequentially by phytochrome B, auxin and hydrogen peroxide in tomato. *Plant Physiology*, **172**, 1259–1272.

Hardtke, C.S., Gohda, K., Osterlund, M.T., Oyama, T., Okada, K. & Deng, X.W. (2000) HY5 stability and activity in *Arabidopsis* is regulated by phosphorylation in its COP1 binding domain. *EMBO Journal*, **19**, 4997–5006.

Heard, N.A., Holmes, C.C., Stephens, D.A., Hand, D.J. & Dimopoulos, G. (2005) Bayesian co-clustering of Anopheles gene expression time series: Study of immune defense response to multiple experimental challenges. *Proceedings of the National Academy of Sciences of the United States of America*, **102**, 16939–16944.

Heyno, E., Innocenti, G., Lemaire, S.D., Issakadis-Bourguet, E. & Krieger-Liszkay, A. (2014) Putative role of the malate valve enzyme NADP-malate dehydrogenase in H_2O_2 signalling in Arabidopsis. *Philosophical Transactions of the Royal Society of London. Series B, Biological Sciences*, **369**, 20130228.

Hoang, N., Schleicher, E., Kacprzak, S., Bouly, J.P., Picot, M., Wu, W. *et al.* (2008) Human and Drosophila cryptochromes are light activated by flavin photoreduction in living cells. *PLoS Biology*, **6**, e160.

Hoecker, U. (2017) The activities of the E3 ubiquitin ligase COP1/SPA, a key repressor in light signalling. *Current Opinion in Plant Biology*, **37**, 63–69.

Holtan, H.E., Bandong, S., Marion, C.M., Adam, L., Tiwari, S., Shen, Y. *et al.* (2011) BBX32, an Arabidopsis B-Box protein, functions in light signalling by suppressing HY5-regulated gene expression and interacting with STH2/BBX21. *Plant Physiology*, **156**, 2109–2123.

Hosseini, P., Tremblay, A., Matthews, B.F. & Alkharouf, N.W. (2010) An efficient annotation and gene-expression derivation tool for Illumina Solexa datasets. *BMC Research Notes*, **3**, 183.

Huang, D.W., Sherman, B.T. & Lempicki, R.A. (2008) Systematic and integrative analysis of large gene lists using DAVID bioinformatics resources. *Nature Protocols*, **4**, 44–57.

Huang, J., Zhao, X. & Chory, J. (2019) The *Arabidopsis* transcriptome responds specifically and dynamically to high light stress. *Cell Reports*, **29**, 4186–4199.

Huang, X., Ouyang, X. & Deng, X.W. (2014) Beyond repression of photomorphogenesis: role switching of COP/DET/FUS in light signalling. *Current Opinion in Plant Biology*, **21**, 96–103.

Jones, M.A., Hu, W., Litthauer, S., Lagarias, J.C. & Harmer, S.L. (2015) A constitutively active allele of phytochrome B maintains circadian robustness in the absence of light. *Physiology*, **169**(1), 814–825.

Kangasjärvi, S., Neukermans, J., Li, S., Aro, E.-M. & Noctor, G. (2012) Photosynthesis, photorespiration, and light signalling in defence responses. *Journal of Experimental Botany*, **63**, 1619–1636.

Karpinski, S., Reynolds, H., Karpinska, B., Wingsle, G., Creissen, G. & Mullineaux, P.M. (1999) Systemic signalling and acclimation in response to excess excitation energy in *Arabidopsis*. *Science*, **284**, 654–657.

Kim, D., Langmead, B. & Salzberg, S.L. (2015) HISAT: a fast-spliced aligner with low memory requirements. *Nature Methods*, **12**, 357–360.

Kleine, T., Kindgren, P., Benedict, C., Hendrickson, L. & Strand, Å. (2007) Genome-wide gene expression analysis reveals a critical role for CRYPTOCHROME1 in the response of Arabidopsis to high irradiance. *Plant Physiology*, **144**, 1391–1406.

Kromdiijk, J., Glowacka, K., Leonelli, L., Gabilly, S.T., Iwai, M., Niyogi, K.K. *et al.* (2016) Improving photosynthesis and crop productivity by accelerating recovery from photoprotection. *Science*, **354**, 857–861.

Lau, K., Podolec, R., Chappuis, R., Ulm, R. & Hothorn, M. (2019) Plant photoreceptors and their signalling components compete for binding to the ubiquitin ligase COP1 using their VP-peptide motifs. *EMBO Journal*, **38**, e102140.

Lau, O.S. & Deng, X.W. (2012) The photomorphogenic repressors COP1 and DET1: 20 years later. *Trends in Plant Science*, **17**, 584–593.

Laubinger, S., Fittinghoff, K. & Hoecker, U. (2004) The SPA quartet: A family of WD-repeat proteins with a central role in suppression of photomorphogenesis in Arabidopsis. *The Plant Cell*, **16**, 2293–2306.

Lawson, T., Davey, P.A., Yates, S.A., Bechtold, U., Baeshen, M., Baeshen, N. *et al.* (2014) C3 photosynthesis in the desert plant *Rhazya stricta* is fully functional at high temperatures and light intensities. *New Phytologist*, **201**, 862–873.

Leivar, P., Monte, E., Oka, Y., Liu, T., Carle, C., Castillon, A. *et al.* (2008) Multiple phytochrome-interacting bHLH transcription factors repress premature seedling photomorphogenesis in darkness. *Current Biology*, **18**, 1815–1823.

Lewis, L.L., Polanski, K., de Torres-Zabala, M., Jayaraman, S., Bowden, L., Moore, J. *et al.* (2015) Transcriptional dynamics driving MAMP-triggered immunity and pathogen effector-mediated immunosuppression in Arabidopsis leaves following infection with *Pseudomonas syringae* pv tomato DC3000. *The Plant Cell*, **27**, 3038–3064.

Li, K., Gao, Z., He, H., Terzaghi, W., Fan, L.-M., Deng, X.W. *et al.* (2015) *Arabidopsis* DET1 represses photomorphogenesis in part by negatively regulating DELLA protein abundance in darkness. *Molecular Plant*, **8**, 622–630.

Li, X., Björkman, O., Shih, C., Grossman, A.R., Rosenquist, M., Jansson, S. *et al.* (2000) A pigment-binding protein essential for regulation of photosynthetic light harvesting. *Nature*, **403**, 391–395.

Li, Z., Wakao, S., Fischer, B.B. & Niyogi, K.K. (2009) Sensing and responding to excess light. *Annual Review of Plant Biology*, **60**, 239–260.

Lian, H.-L., He, S.-B., Zhang, Y.-C., Zhu, D.-M., Zhang, J.Y., Jia, K.-P. *et al.* (2011) Blue-light-dependent interaction of cryptochrome 1 with SPA1 defines a dynamic signaling mechanism. *Genes & Development*, **25**, 1023–1028.

Liu, Q., Su, T., He, W., Ren, H., Liu, S., Chen, Y. *et al.* (2020) Photooligomerization determines photosensitivity and photoreactivity of plant cryptochromes. *Molecular Plant*, **13**, 398–413.

Long, S.P., Humphries, S. & Falkowski, P.G. (1994) Photoinhibition of photosynthesis in nature. *Annual Review of Plant Biology*, **45**, 633–662.

Love, M.I., Huber, W. & Anders, S. (2014) Moderated estimation of fold change and dispersion for RNA-seq data with DESeq2. *Genome Biology*, **15**, 550.

Mittler, R., Vanderauwera, S., Gollery, M. & Van Breusegem, F. (2004) Reactive oxygen network of plants. *Trends in Plant Science*, **9**, 490–498.

Moriyama, E.N., Strope, P.K., Opiyo, S.O., Chen, Z. & Jones, A.M. (2006) Mining the *Arabidopsis thaliana* genome for highly-divergent seven transmembrane receptors. *Genome Biology*, **7**, R96.

Mullineaux, P.M., Exposito-Rodriguez, M., Laissue, P.P. & Smirnoff, N. (2018) ROS-dependent signaling pathways in plants and algae exposed to high light: Comparisons with other eukaryotes. *Free Radical Biology and Medicine*, **122**, 52–64.

Murchie, E.H. & Horton, P. (1997) Acclimation of photosynthesis to irradiance and spectral quality in British plant species: chlorophyll content, photosynthetic capacity and habitat preference. *Plant, Cell and Environment*, **20**, 438–448.

Murchie, E.H., Hubbert, S., Peng, S. & Horton, P. (2005) Acclimation of photosynthesis to high irradiance in rice: gene expression and interactions with leaf development. *Journal of Experimental Botany*, **56**, 449–460.

Naznin, M.T., Lefsrud, M., Gravel, V. & Azad, M.O.K. (2019) Blue light added with red LEDS enhance growth characteristics, pigments content, and antioxidant capacity in lettuce, spinach, kale, Basil and sweet pepper in a controlled environment. *Plants*, **8**, 93.

Oguchi, R., Hikosaki, K. & Hirose, T. (2003) Does the photosynthetic light-acclimation need change in leaf anatomy? *Plant, Cell and Environment*, **26**, 505–512.

Overmyer, K., Köllist, H., Tuominen, H., Betz, C., Langebartels, C., Wingsle, G. *et al.* (2008) Complex phenotypic profiles leading to ozone sensitivity in *Arabidopsis thaliana* mutants. *Plant, Cell and Environment*, **31**, 1237–1249.

Oyama, T., Shimura, Y. & Okada, K. (1997) The *Arabidopsis HY5* gene encodes a bZIP protein that regulates stimulus-induced development of root and hypocotyl. *Genes & Development*, **11**, 2983–2995.

Park, H.-Y., Lee, S.-Y., Seok, H.-Y., Kim, S.-H., Sung, Z.R. & Moon, Y.-H. (2011) EMF1 interacts with EIP1, EIP6 or EIP9 involved in the regulation of flowering time in Arabidopsis. *Plant and Cell Physiology*, **52**, 1376–1388.

Penfold, C.A. & Buchanan-Wollaston, V. (2014) Modelling transcriptional networks in leaf senescence. *Journal of Experimental Botany*, **65**, 3859–3873.

Penfold, C.A. & Wild, D.L. (2011) How to infer gene networks from expression profiles, revisited. *Interface Focus*, **1**, 857–870.

Pham, V.C., Xu, X. & Huq, E. (2018) Molecular bases for the constitutive photomorphogenic phenotypes in *Arabidopsis*. *Development*, **145**, dev169870.

Piasecka, A., Jedrzejczak-Rey, N. & Bednarek, P. (2015) Secondary metabolites in plant innate immunity: conserved function of divergent chemicals. *New Phytologist*, **206**, 948–964.

Ramel, F., Birtic, S., Ginies, C., Soubigopu-Taconnat, L., Triantaphylidès, S. & Havaux, M. (2012) Carotenoid oxidation products are stress signals that mediate gene responses to singlet oxygen in plants. *Proceedings of the National Academy of Sciences of the United States of America*, **109**, 5535–5540.

Ramel, F., Ksas, B., Akkari, E., Mialoundama, A.S., Monnet, F., Krieger-Liszkay, A. *et al.* (2013) Light-induced acclimation of the *Arabidopsis chlorina1* mutant to singlet oxygen. *The Plant Cell*, **25**, 1445–1462.

Reed, J., Nagatani, A., Elich, T., Fagan, M. & Chory, J. (1994) Phytochrome A and phytochrome B have overlapping but distinct functions in Arabidopsis development. *Plant Physiology*, **104**, 1139–1149.

Ruban, A.V. & Belgio, E. (2014) The relationship between maximum tolerated light intensity and photoprotective energy dissipation in the photosynthesis antenna: chloroplast gains and losses. *Philosophical Transactions of the Royal Society of London. Series B, Biological Sciences*, **369**, 20130222.

Ruckle, M.E., DeMarco, S.M. & Larkin, R.M. (2007) Plastid signals remodel light signalling networks and are essential for efficient chloroplast biogenesis in *Arabidopsis*. *The Plant Cell*, **19**, 3944–3960.

Schiebe, R. (2004) Malate valves to balance cellular energy supply. *Physiologia Plantarum*, **120**, 21–26.

Schiebe, R. & Dietz, K.-J. (2012) Reduction-oxidation network for flexible adjustment of cellular metabolism in photoautotrophic cells. *Plant, Cell and Environment*, **35**, 202–216.

Schottler, M.A. & Toth, S.Z. (2014) Photosynthetic complex stoichiometry dynamics in higher plants: environmental acclimation and photosynthetic flux control. *Frontiers in Plant Science*, **5**, 188.

Sclep, G., Allemeersch, J., Liechti, R., De Meyer, B., Beynon, J., Bhalerao, R. *et al.* (2007) CATMA, a comprehensive genome-scale resource for silencing and transcript profiling of Arabidopsis genes. *BMC Bioinformatics*, **8**, 400.

Shaikhali, J., Barajas-Lopéz, J.D., Ötvös, K., Kremnev, D., Garcia, A.S., Srivastava, V. *et al.* (2012) The CRYPTOCHROME1-dependent response to excess light is mediated through the transcriptional activators ZINC FINGER PROTEIN EXPRESSED IN INFLORESCENCE MERISTEM LIKE1 and ZML2 in *Arabidopsis*. *The Plant Cell*, **24**, 3009–3025.

Shannon, P., Markiel, A., Ozier, O., Baliga, N.S., Wang, J.T., Ramage, D. *et al.* (2003) Cytoscape: a software environment for integrated models of biomolecular interaction networks. *Genome Research*, **13**, 2498–2504.

Shikata, H., Hanada, K., Ushijima, T., Nakashima, M., Suzuki, Y. & Matsushita, T. (2014) Phytochrome controls alternative splicing to mediate light responses in *Arabidopsis*. *Proceedings of the National Academy of Sciences of the United States of America*, **111**, 18781–18786.

Stegle, O., Denby, K.J., Cooke, E.J., Wild, D.L., Ghahramani, Z. & Borgwardt, K.M. (2010) A robust Bayesian two-sample test for detecting intervals of differential gene expression in microarray time series. *Journal of Computational Biology*, **17**, 355–367.

Streb, P., Josse, E.-M., Gallouët, E., Baptist, F., Kuntz, M. & Cornic, G. (2005) Evidence for alternative electron sinks to photosynthetic carbon assimilation in the high mountain plant species *Ranunculus glacialis*. *Plant, Cell and Environment*, **28**, 1123–1135.

Suorsa, M., Järvi, S., Grieco, M., Nurmi, M., Pietrzykowska, M., Rantala, M. *et al.* (2012) PROTON GRADIENT REGULATION5 is essential for proper acclimation of *Arabidopsis* photosystem I to naturally and artificially fluctuating light conditions. *The Plant Cell*, **24**, 2934–2948.

Terashima, I., Hanba, Y.T., Tholen, D. & Niinemets, Ü. (2011) Leaf functional anatomy in relation to photosynthesis. *Plant Physiology*, **155**, 108–116.

Toledo-Ortiz, G., Huq, E. & Quail, P.H. (2003) The Arabidopsis Basic/Helix-Loop-Helix transcription factor family. *The Plant Cell*, **15**, 1749–1770.

Toledo-Ortiz, G., Johansson, H., Lee, K.P., Bou-Torrent, J., Stewart, K., Steel, G. *et al.* (2014) The HY5-PIF regulatory module coordinates light and temperature control of photosynthetic gene transcription. *PLOS Genetics*, **10**, e1004416.

Triantaphyllidès, C., Krischke, M., Hoeberichts, F.A., Ksas, B., Gresser, G., Havaux, M. *et al.* (2008) Singlet oxygen is the major reactive oxygen species involved in photooxidative damage to plants. *Plant Physiology*, **148**, 960–968.

Tripathi, P., Carvallo, M., Hamilton, E.E., Preuss, S. & Kay, S.A. (2017) *Arabidopsis* B-BOX32 interacts with CONSTANS-LIKE3 to regulate flowering. *Proceedings of the National Academy of Sciences of the United States of America*, **114**, 172–177.

Underwood, W. (2012) The plant cell wall: a dynamic barrier against pathogen invasion. *Frontiers in Plant Science*, **3**, 85.

Van Acken, O. & Whelan, J. (2012) Comparison of transcriptional changes to chloroplast and mitochondrial perturbations reveals common and specific responses in Arabidopsis. *Frontiers in Plant Science*, **3**, 291.

van Rooijen, R., Aarts, M.G.M. & Harbinson, J. (2015) Natural genetic variation for acclimation of photosynthetic light use efficiency to growth irradiance in Arabidopsis. *Plant Physiology*, **167**, 1412–1429.

Vialet-Chabrand, S., Matthews, J.S.A., Simkin, A.J., Raines, C.A. & Lawson, T. (2017) Importance of fluctuations in light on plant photosynthetic acclimation. *Plant Physiology*, **173**, 2163–2179.

Walters, R.G., Rogers, J.J.M., Shephard, F. & Horton, P. (1999) Acclimation of *Arabidopsis thaliana* to the light environment: the role of photoreceptors. *Planta*, **209**, 517–527.

Waters, M.T., Wang, P., Korkaric, M., Capper, R.G., Saunders, N.J. & Langdale, J.A. (2009) GLK transcription factors coordinate expression of the photosynthetic apparatus in *Arabidopsis*. *The Plant Cell*, **21**, 1109–1128.

Willems, P., Mhamdi, A., Stael, S., Storme, V., Kerchev, P., Noctor, G. *et al.* (2016) The ROS wheel: Refining transcriptional footprints. *Plant Physiology*, **171**, 1720–1733.

Windram, O. & Denby, K.J. (2015) Modelling signalling networks underlying plant defence. *Current Opinion in Plant Biology*, **27**, 165–171.

Windram, O., Madhou, P., McHattie, S., Hill, C., Hickman, R., Cooke, E. *et al.* (2012) Arabidopsis defense against *Botrytis cinerea*: Chronology and regulation deciphered by high-resolution temporal transcriptomic analysis. *The Plant Cell*, **24**, 3530–3557.

Wingler, A., Lea, P.J., Quick, W.P. & Leegood, R.C. (2000) Photorespiration: metabolic pathways and their role in stress protection. *Philosophical Transactions of the Royal Society of London. Series B, Biological Sciences*, **355**, 1517–1529.

Wituszyńska, W., Ślesak, I., Vanderauwera, S., Szechyńska-Hebda, M., Kornaś, A., Van Der Kelen, K. *et al.* (2013) *LESION SIMULATING DISEASE1, ENHANCED DISEASE SUSCEPTIBILITY1*, and *PHYTOALEXIN DEFICIENT4* conditionally regulate cellular signaling homeostasis, photosynthesis, water use efficiency, and seed yield in Arabidopsis. *Plant Physiology*, **161**, 1795–1805.

Wu, H., Kerr, K., Cui, X. & Churchill, G. (2003) MAANOVA: A software package for the analysis of spotted cDNA microarray experiments. In: Parmigiani, G., Garrett, E., Irizarry, R. & Zeger, S. (Eds.) *The Analysis of Gene Expression Data: Methods and Software*. New York: Springer, pp. 313–341.

Xu, D., Li, J., Gangappa, S.N., Hettiarachchi, C., Lin, F., Andersson, M.X. *et al.* (2014) Convergence of light and ABA signalling on the *ABI5* promoter. *PLOS Genetics*, **10**, e1004197.

Yoshida, Y., Sarmiento-Manus, R., Yamori, W., Ponce, M.R., Micol, J.L. & Tsukaya, H. (2018) The Arabidopsis *phyB-9* mutant has a second-site mutation in the *VENOSA4* gene that alters chloroplast size, photosynthetic traits, and leaf growth. *Plant Physiology*, **178**, 3–6.

Yu, X., Liu, H., Klejnot, J. & Lin, C. (2010) The cryptochrome blue light receptors. *The Arabidopsis Book*, **8**, e0135.